

AD-A101 945

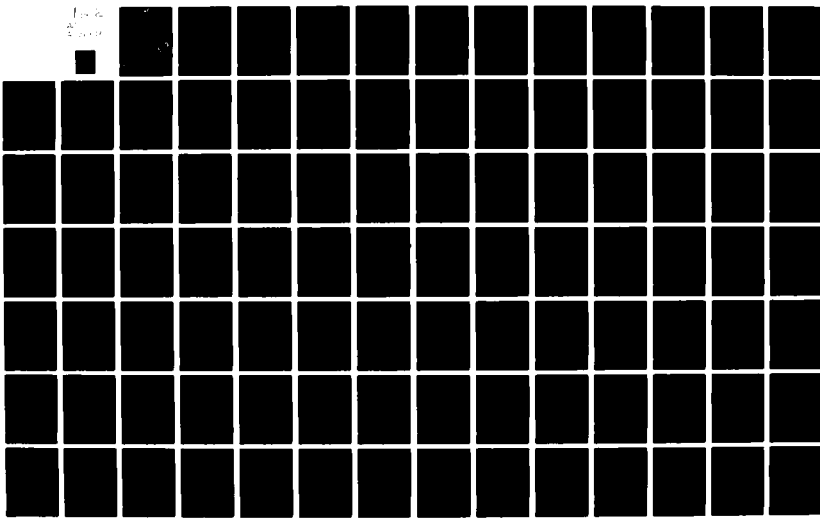
ILLINOIS UNIV AT URBANA DEPT OF PHYSICS
ELECTRONIC STRUCTURE OF SOLIDS AND THEIR SURFACES AND INTERFACE--ETC(U)
JUN 81 A B KUNZ AFOSR-76-2989

F/G 20/12

NL

UNCLASSIFIED

AFOSR-TR-81-0571



DTIC FILE COPY

AD A101945

unclassified

LEVEL I 13

SECURITY CLASSIFICATION OF THIS PAGE (When Data Entered)

14) REPORT DOCUMENTATION PAGE		READ INSTRUCTIONS BEFORE COMPLETING FORM
1. REPORT NUMBER AFOSR/TR. 81-0571	2. GOVT ACCESSION NO. AD-A101945	3. RECIPIENT'S CATALOG NUMBER
4. TITLE (and Subtitle) ELECTRONIC STRUCTURE OF SOLIDS AND THEIR SURFACES AND INTERFACES	5. TYPE OF REPORT & PERIOD COVERED Final Scientific Report 04-01-80/06-30-81	
6. PERFORMING ORG. REPORT NUMBER	7. AUTHOR(s) A. B. Kunz	8. CONTRACT OR GRANT NUMBER(s) AFOSR-76-2989
9. PERFORMING ORGANIZATION NAME AND ADDRESS Department of Physics, Loomis Lab. of Physics University of Illinois at Urbana-Champaign 1110 West Green St. Urbana, IL 61801	10. PROGRAM ELEMENT, PROJECT, TASK AREA & WORK UNIT NUMBERS 2306/32 611025	
11. CONTROLLING OFFICE NAME AND ADDRESS Air Force Office of Scientific Research Bolling Air Force Base, D.C. 20332	12. REPORT DATE 06-30-81	
14. MONITORING AGENCY NAME & ADDRESS(if different from Controlling Office)	13. NUMBER OF PAGES 140	
	15. SECURITY CLASS. (of this report) Unclassified	
	15a. DECLASSIFICATION/DOWNGRADING SCHEDULE	
16. DISTRIBUTION STATEMENT (of this Report) A - Approved for public release; distribution is unlimited.		
17. DISTRIBUTION STATEMENT (of the abstract entered in Block 20, if different from Report)		
18. SUPPLEMENTARY NOTES		
19. KEY WORDS (Continue on reverse side if necessary and identify by block number) Band Structure Interfaces Shallow Impurities Semiconductors (polar) Deep Impurities Surfaces		
20. ABSTRACT (Continue on reverse side if necessary and identify by block number) The past five years of this project have been devoted to development of qualitative theories of the fundamental electronic structure of pure and impure semiconductors. The basic theoretical tools and also conclusions relating to chiefly photoemission type experiments and to some extent spectroscopy of pure II-VI and III-V compounds are presented in Chapters 1 and 2 of this report. Basic complete work relating to adsorbates and their spectra are reported in Chapter 3. Several related studies are being completed at this point and several articles relating to these studies are being prepared for publication.		

DD FORM 1 SEP 73 1473 EDITION OF 1 NOV 65 IS OBSOLETE

unclassified
SECURITY CLASSIFICATION OF THIS PAGE (When Data Entered)S DTIC ELECTRONIC
C JUL 24 1981

Final Scientific Report

Grant AFOSR-76-2989

**A. Barry Kunz, Professor of Physics
Principal Investigator**

**Department of Physics
University of Illinois at Urbana-Champaign
Urbana, IL 61801**

**Project terminated 31 March 1981
Report submitted June 1981**

**Approved for public release;
distribution unlimited.**

817 24 009

Table of Contents

<u>Page</u>
1 Introduction
2 Chapter 1, Theory of Energy Bands in II-VI Compounds
79 Chapter 2, Ab Initio Energy Bands and Ionization Energies for ALP, GaP and GaAs
98 Chapter 3, Surface Adsorbate Spectroscopy
135 Appendix 1 Post Doctoral Associates Supported by this Grant
136 Appendix 2 Graduate Students Supported by this Grant
137 Appendix 3 Publications Supported by this Grant

Accession For	
NTIS GRA&I	<input checked="" type="checkbox"/>
DTIC TAB	<input type="checkbox"/>
Unannounced	<input type="checkbox"/>
Justification	
By _____	
Distribution/	
Availability Codes	
Avail and/or	
Dist	Special
A	

AIR FORCE OFFICE OF SCIENTIFIC RESEARCH (AFSC)
NOTICE OF TRANSMITTAL TO DDC
This technical report has been reviewed and is
approved for public release IAW AFR 190-12 (7b).
Distribution is unlimited.
A. D. BLOSE
Technical Information Officer

Introduction

The past five years of this project have been devoted to development of qualitative theories of the fundamental electronic structure of pure and impure semiconductors. The basic theoretical tools and also conclusions relating to chiefly photoemission type experiments and to some extent spectroscopy of pure II-VI and III-V compounds are presented in Chapters 1 and 2 of this report. Basic complete work relating to adsorbates and their spectra are reported in Chapter 3. Several related studies are being completed at this point and several articles relating to these studies are being prepared for publication.

Chapter 1.

Theory of Energy Bands in II-VI Compounds.

Introduction

This investigation has the purpose of performing self-consistent energy band calculations on some of the II-VI compounds, such as cadmium sulfide, zinc oxide, and zinc sulfide.

There are many practical and theoretical reasons for interest in these materials.

These materials have applications as phosphors (ZnS and CdS), as infrared detectors (ZnS), in photovoltaic cells ($CdS-Cu_2S$ or $CdS-CdTe$ heterojunctions), in batteries (ZnO), as FETs (CdS), in heterojunction lasers (CdS), and even as acoustic amplifiers (CdS).

They are of considerable theoretical interest as well, as examples of wide band gap solids, intermediate between the covalent III-V semiconductors and the more ionic I-VII insulators. They serve as a test of calculational methods previously used on the lighter III-V compounds and other compounds simpler than these II-VI compounds.

In particular, the occupied d-levels, which lie in energy near the top of the valence levels, complicate the picture. The positions of the d-bands have not been correctly predicted in previous ab initio calculations, and in fact some methods fail qualitatively by not obtaining the proper ordering of the valence s,p and d levels.

The II-VI compounds have also been of theoretical interest as excitonic systems. High densities of such electron-hole complexes have been produced and observed in CdS. The electron-hole liquid has been observed and studied in CdS as well.

In addition, some very interesting magnetic properties in CuCl and CdS have recently been observed. This is the background of these experimental studies. Anomalous diamagnetism has been observed in CuCl under rapid pressure and temperature cycling. In some samples, up to 50% of the magnetic flux is excluded. This occurs at high temperatures (150 K!) and cannot be explained by ordinary diamagnetism. The only currently known phenomenon that can explain this is superconductivity.

9

It's clear that this would have to be superconductivity of different origin. Acoustic phonons, the known mechanism, are too low in energy to bind electrons at such high temperatures. Models using some other form of interaction to pair electrons seem to be necessary. Some form of excitonic binding is proposed in many of these models. One of the most well-known such models, the Allender-Bray-Bardeen model, requires a metal and a semiconductor to exist in very close proximity. Since CuCl can disproportionate via the reaction $2\text{CuCl} \rightarrow \text{Cu} + \text{CuCl}_2$, this model has appealed to many. However, cadmium sulfide, which has been observed to have only one valence state and is not believed to disproportionate, has shown similar anomalous diamagnetism. The law of parsimony is, therefore, against the metal-semiconductor sandwich idea. Also, in both CuCl and CdS, impurities clearly play a major role. Sufficiently clean samples display no interesting behaviour at all. And to make life even more interesting, cadmium sulfide also becomes a ferromagnet under a high (40 kilogauss) applied field.

5

Another model, proposed by Bishop and Overhauser (), involves the interaction mediated by the optical phonons. This mechanism has deep attractive potential wells, about 10 mev in depth for a spacing of 250 angstroms. This suggests the possibility of bound states, and the pairing is considerably stronger, around a factor of ten, than the pairing from acoustic phonons in the typical Cooper pair in the highest temperature superconductors known, at approximately 20 degrees Kelvin. This idea is even more intriguing in the light of the fact that both CdS and CuCl are strongly polar compounds. This suggest that these phenomena would not be seen in the less polar III-V compounds and in elemental semiconductors such as Ge and Si. They've been investigated most thoroughly and indeed, such effects have not been observed.

Chapter One

The calculations discussed here are based on Hartree-Fock theory, the most common approximation to the exact non-relativistic theory of a many-electron system. I'll discuss the theory and its applications to crystalline solids. The specialization of Hartree-Fock theory used in these calculations, the method of local orbitals, deserves and gets a chapter of its own.

The original problem is finding exact solutions to the Schrodinger equation for a many-electron system. This is impossible, if the universe is as small as we think it is. Consider the wavefunction, which is a $3N$ dimensional function if there are N electrons. Dividing each axis into, say, 100 units, in order to numerically integrate and differentiate, we need to record 10^{6N} entries. The same problem arises if we try to describe the wavefunction by

sets of orthogonal functions. 10^{6N} is just too big a number.

Quantum mechanics is against us. The upper limit for the rate of information flow in a computer of mass M is Mc^2/h (h = Planck's constant, c = speed of light), in bits per second. It's not hard to see that macroscopic physical systems cannot be exactly simulated by digital computers. I emphasize the word digital, since the electron is an excellent analog of itself.

Such a digital simulation would be useless even if it could be done. As suggested, the real solid simulates itself perfectly. The goal of physics is to explain some set of occurrences in terms of a few, relatively simple ideas, rather than making a model isomorphic with the universe and just as confusing.

We begin to clear away some complications by using the Born-Oppenheimer approximation. This neglects any relationship between the motion of the electrons and the motion of the nuclei. This a valid simplification, since

the nuclei range from 10^3 to 10^5 times heavier than an electron.

We can express the N -electron wavefunction as a function of the electronic coordinates alone:

$$\Psi_N = \Psi_N(x_1, x_2, \dots, x_N) \quad (1.1)$$

Here Ψ_N contains the position and spin coordinates of the i th electron. We write the Schrodinger equation for this wavefunction:

$$H \Psi_N(x_1, x_2, \dots, x_N) = E_N \Psi_N(x_1, x_2, \dots, x_N) \quad (1.2)$$

Here, H is the non-relativistic Hamiltonian expressed in atomic units. In this system of units, $\hbar = 1$, $c = 2$, and the mass of the electron is one-half. The unit of distance is one bohr (.529 angstroms) and the unit of energy is the rydberg (13.6 ev).

$$H = H_e + H_n + H_{int} \quad (1.3)$$

and

$$\begin{aligned} H_e &= -\sum_i \nabla_i^2 + \sum_{i \neq j} \frac{1}{|\vec{r}_i - \vec{r}_j|} \\ H_n &= -\sum_I \frac{1}{M_I} \nabla_I^2 + \sum_{I, J} Z_I Z_J \frac{1}{|\vec{R}_I - \vec{R}_J|} \\ H_{int} &= -2 \sum_I \sum_x \frac{1}{|\vec{r}_x - \vec{R}_I|} \end{aligned} \quad (1.4)$$

H_n is independent of the electron coordinates, and has been assumed to be a constant, as per the Born-Oppenheimer approximation.

The upper case characters refer to nuclear properties: Z is the atomic number, R is the nuclear position (usually assumed to be fixed, like Fimlico) and M is the nuclear mass. The lower case characters describe properties of the electrons. x_i is the coordinate of the ith electron.

The atomic numbers of the atoms under consideration are relatively low, and since in any event it is the valence electrons that are of primary interest, the non-relativistic nature of the Hamiltonian may be acceptable.

The fundamental approximation, now applied, is the independent particle model. In truth, in the real solution, the variables are not separable. We must assume that they are, or more exactly that the true wavefunction can be well-approximated by this model. The independent particle model says that the electron is acted on by the average of the other electrons. The N-electron wavefunction is expressed as a product of one-electron wavefunctions, or as a linear combination of such products. A simple example is the Hartree wavefunction:

$$\Psi_N = \psi_1(x_1) \psi_2(x_2) \cdots \psi_N(x_n) \quad (1.5)$$

Since electrons are fermions, this N-electron wavefunction must be antisymmetric. Any interchange of two particles must reverse the sign of the wavefunction. The simplest way to antisymmetrize is to use the determinant of a matrix whose elements are

spinorbitals.

$$\psi_N = (N!)^{\frac{1}{2}} \text{Det}$$

$$\begin{bmatrix} \theta_1(x_1) \theta_1(x_2) \dots & \theta_1(x_N) \\ \theta_2(x_1) \theta_2(x_2) \dots & \\ \vdots & \vdots \\ \theta_N(x_1) \dots & \theta_N(x_N) \end{bmatrix} \quad (1.6)$$

Not all such ψ_N are spin eigenstates, but fortunately we have here closed-shell systems that can be expressed as single-determinantal wavefunctions.

For any arbitrary ψ_N , we can find the expectation value of the Hamiltonian. It is a sum of one- and two-particle integrals:

$$\langle \psi_N | H | \psi_N \rangle = \sum_{i=1}^N \langle i | f_{0i} | i \rangle + \sum_{i,j=1}^N \langle i, j | g_{ij} (1 - P_{ij}) | i, j \rangle \quad (1.7)$$

$$| i, j \rangle = \theta_i(x_i) G_j(x_j) \quad (1.8)$$

P is a permutation operator, constructed so that

$P_{ij} | i, j \rangle = | j, i \rangle$. The terms $i=j$ are not a problem since the self-energy cancels the 'self-exchange'.

The expectation value of the Hamiltonian, $\langle \psi_n | H | \psi_n \rangle$, can be minimized by varying the spinorbitals. It has been shown that

$$\frac{\langle \psi_n | H | \psi_n \rangle}{\langle \psi_n | \psi_n \rangle} \geq E \quad (1.9)$$

where E is the energy of the exact ground state.

We vary the orbitals, but take care to keep them orthogonal, for convenience and without loss of generality. This is done by using Lagrange multipliers. The objective is to obtain the lowest upper bound to the exact non-relativistic energy.

We define the functional

$$L = \langle \psi_n | H | \psi_n \rangle - \sum_{i,j=1}^N \lambda_{ij} (\langle \psi_i | \psi_j \rangle - \delta_{ij}) \quad (1.10)$$

and require that the variation of $L = 0$ for $i = 1, 2, \dots, N$.

This yields a set of N coupled nonlinear integrodifferential equations known as the Hartree-Fock equations.

$$\left\{ -\nabla^2 - \sum_j \frac{2z_j}{|R_j - R|} + 2 \sum_{j=1}^N (J_j - K_j) \right\} \Theta_i(x) = \sum_{j=1}^N \lambda_{ij} \Theta_j(x) \quad (1.11)$$

J_j and K_j have the familiar Coulomb and exchange operator forms.

$$J_j \Theta_i(x) = \left\{ \int \frac{1 \Theta_j(x')}{|R - R'|} d^3x' \right\} \Theta_i(x) \quad (1.12)$$

$$K_j \Theta_i(x) = \left\{ \int \frac{\Theta_j^*(x') \Theta_i(x')}{|R - R'|} d^3x' \right\} \Theta_i(x) \quad (1.13)$$

These equations may be written in matrix form;

$$F \Theta = SG \quad (1.14)$$

F is the $N \times N$ matrix of the Fock operator. For closed shells, it is Hermitian, so S may be diagonalized by a unitary transformation. Fortunately, the II-VI compounds have closed shells. We may write, $F |i\rangle = E_i |i\rangle$. (1.15)

Combining this expression with equation 1.7 gives the Hartree-Fock ground state energy,

$$E_{HF}^N = (1/2) \sum_i \{ E_i + \langle \psi_i | f | i \rangle \} . \quad (1.16)$$

The E_i 's are the single-particle energies, almost. Koopman's theorem states that given a variationally stationary state formed from N simultaneous spinorbital (pseudo)eigenfunctions of the N particle Fock operator F , the states ψ_{N+1} and ψ_{N-1} , formed by altering the list of occupied eigenfunctions of F by one entry, are stationary with respect to further variation of that spinorbital whose occupancy has been altered. If we neglect relaxation effects, E_i is the entire change in system energy when an electron is added or removed.

In order to equate the E_i 's with single-particle energies, we must also assume that relaxation effects are small - that the other occupied orbitals change only slightly when an

There are such changes, since the Fock operator is a functional of all of its own solutions, and changing one of them must change all. The question is, how much? These relaxation effects will be discussed in a later section.

The Method of Local Orbitals

The method of local orbitals is a variational technique in which solutions to the Hartree-Fock equations are sought for a small subsystem of the system of interest, with the caveat that all such solutions found must be contained within the occupied Fock space of the original system. Sets of such local orbitals, which are not orthogonal, can then be assigned to each subunit of the larger system using the translational invariance of the Fock-Dirac density matrix, thus spanning the occupied Hilbert space of that system.

A single noniterative rotation of the local orbitals within this occupied space then yields the exact self-consistent solutions for the original Fock operator.

If $\{\theta_i\}_{i=1}^n$ is the set of local orbitals satisfying the Hartree-Fock equations for an n-electron system, then $F\theta_i = \sum_j \lambda_j \theta_j$ (3.1)

The Fock-Dirac density operator for the equation is

$$\rho = \sum_{i,j} \theta_i S_{ij}^{-1} \theta_j^T \quad (3.2)$$

S^{-1} is the inverse of the overlap matrix S.

$$S_{ij}^{-1} = \int \theta_i^*(x) \theta_j(x) d^3x \quad (3.3)$$

Rho (ρ) is a projection operator ($\rho^2 = \rho$ and $\rho = \rho^T$)

chosen such that $\rho \theta_i = \theta_i$ for any orbital θ_i in the occupied space

and $\rho \chi = 0$ for any orbital χ in the virtual space. This means

that for any one-electron operator L, the projection of L

onto the Hartree-Fock manifold will satisfy

$$\rho L \rho \theta_i = \sum_j Y_{ij} \theta_j \quad (3.4)$$

for any occupied orbital θ_i , and $\rho L \rho \chi = 0$ for any virtual orbital χ .

Another approach, rigorously developed by Gilbert (),

begins by introducing modified Hartree-Fock equations of the form

$$(F + \rho A \rho) \theta_i' = E_i' \theta_i' \quad (3.5)$$

Above, A is an as yet unspecified Hermitian operator and rho

is the 'diagonal' (x equals x prime) form of the Fock-Dirac

density operator (). We see that rho is idempotent, Hermitian,

and projects onto occupied Fock space. Because of this last

property, it can be shown that the occupied eigenfunctions of

the modified Hartree-Fock equation lie entirely within the occupied Fock space of the unmodified Hartree-Fock equations.

$$\text{So, } \rho \theta_i' = \begin{cases} \theta_i' & \text{if } \theta_i' \text{ is occupied} \\ 0 & \text{otherwise} \end{cases} \quad (3.6)$$

There is no Koopman's theorem for this modified equation, and so the ξ_i 's cannot be interpreted as being nearly the particle energies, as they can in the regular Hartree-Fock equations. The total energy of the subsystem still has significance since a unitary transformation within occupied Fock space leaves the trace of Hermitian operators such as the Hamiltonian invariant.

The properties of the θ_i 's will vary with the choice of A . We are looking for functions that are localized on specific lattice sites of a crystal. In order to decide which operator best fulfills such a purpose, we need to consider the minimization of a functional $\mathcal{J}[\theta_1, \theta_2, \dots, \theta_N]$

subject to the variational constraints $\langle i | \rho - \langle i | = 0$;

$$\rho |i\rangle - |i\rangle = 0; \langle i | j \rangle - \delta_{ij} = 0 \quad (3.7)$$

Since we can use the method of Lagrange multipliers, The integral

constraints of equation 3.7 are taken into account by the parameters λ_{ij} , and the constraints that involve explicit functions of X in equation 3.7 are taken care of by Lagrange functions $\eta_i(x)$ and $\eta'_i(x)$.

We obtain

$$\begin{aligned} & \delta_k^+ \{ \mathcal{D}[\theta] - \sum_{i,j=1}^N \lambda_{ij} (\langle i|j \rangle - \delta_{ij}) \} \\ & - \sum_{i=1}^N \eta_i(x) (\langle i|j \rangle - \langle i|i \rangle) - \sum_{i=1}^N \eta'_i(x) (\langle j|i \rangle - \langle i|j \rangle) \quad (3.8) \\ & = \delta_k^+ \mathcal{D}[\theta] - \sum_{j=1}^N \lambda_{kj} |j\rangle - \eta_k(x) j + \eta'_k(x) = 0 \end{aligned}$$

Multiplying on the left by $(1-p)$, we see

$$(1-p)|j\rangle = 0 \quad j=1, 2, \dots, N \quad (3.9)$$

$$\text{and } (1-p)\eta_k j = \{(1-p)\eta_k\} j = 0 \text{ for all } \eta_k \quad (3.10)$$

$$\text{and so } \delta_k^+ \mathcal{D}[\theta] + \eta'_k(x) = p \left(\sum_k^+ \mathcal{D}[\theta] - \eta_k(x) \right) \quad (3.11)$$

Substituting equation 3.11 into 3.8, we get

$$p \delta_k^+ \mathcal{D}[\theta] = \sum_{j=1}^N \lambda_{kj} |j\rangle \quad (3.12)$$

$$\text{which may be rewritten as } G|k\rangle = \sum_{j=1}^N \lambda_{kj} |j\rangle \quad (3.13)$$

$$\text{where } G = p \sum_{i,j=1}^N (\delta_i^+ \mathcal{D}) \sum_j^+ \langle ji | = G^+ \quad (3.14)$$

A unitary transformation gives

$$G|k'\rangle = E'_k |k'\rangle \quad (3.15)$$

Since we now know how to minimize any chosen Hermitian

functional \mathcal{J} , we can now get back to the true problem. Let

$$A = G - F, \text{ so that } [(F + \rho A_p), G] = 0 \quad (3.16)$$

We can now minimize \mathcal{J} and solve equation 3.5 at the same time,

and so may pick A to satisfy physical reasoning.

We choose A so that the solutions are localized on a site,

usually by picking A to be some potential well centered on the

site. The Fock operator can be separated into F_s , the atomic

Fock operator for the site s , and U_s , an external potential

operator for the site s . We usually pick the localizing potential,

A , to be $-U_s$. The local orbitals equation is now

$$[F_s + U_s - \rho V_{sj}] \theta_{si} = \epsilon_{si} \theta_{si} \quad (3.17)$$

This isn't an obvious improvement over the original Hartree-Fock equation, but it allows a systematic approximation

that simplifies greatly the Hartree-Fock problem without inducing

undue error. The left side of equation 3.17 can be analyzed by

the order of the intersite overlap. The Fock-Dirac density

operator is $\rho = \sum_{si} \sum_{Tj} \theta_{si} V_{si,Tj} \theta_{Tj}^*$ (3.18)

with V the interatomic overlap matrix.

$$V_{s_i \bar{t}_j} = \int \theta_{s_i}^*(x) \theta_{\bar{t}_j}(x) dx \quad (3.19)$$

As discussed in Lowdin (), $V_{s_i \bar{t}_j}$ may be expanded in a power

$$\text{series in } V_{s_i \bar{t}_j}: V_{s_i \bar{t}_j} = V_{s_i \bar{t}_j} - V_{s_i \bar{t}_j} + \dots \quad (3.20)$$

Expanding the local orbitals equation and discarding second order and greater in intersite overlap () gives

$$[F_s + U'_s - g_s U'_s P_s] \theta_{s_i} = E'_{s_i} \theta_{s_i} \quad (3.21)$$

where $P_s = \sum_{ij} \theta_{s_i} \theta_{s_j}^\dagger$ and

$$U'_s = \sum_{T \neq s} \left\{ -2 Z_T \frac{1}{|R_T - r|} + 2 \sum_j \int \frac{|\theta_{t_j}(x)|^2 dx'}{|r - r'|} \right\}$$

As self-consistency is approached, the last two terms of equation 3.21 tend to cancel. Therefore, the Fock space rotation changes Bloch wavefunctions into atomic-like wavefunctions that are eigenfunctions of the atomic Fock operator.

We proceed to localize a physically realistic number of electrons on each site. In cadmium sulfide, we choose to have 46 electrons on the cadmium site and 18 on the sulfur, approximating an ionic charge distribution (overlap and diffuse valence orbitals permit complete covalency if needed, however).

We have achieved several advantages. The problem is computationally simplified, since the equation being iterated

does not have to portray the full complexities of the solid, and since the local orbitals are recognizably modified atomic orbitals and aid in picturing chemical bonding. This approach has use as a beginning in looking at amorphous substances, which have only a short-range order.

The local orbitals are calculated using the program called LOPAS written by Kunz. A basis function expansion of Slater orbitals (STOs) is used for the radial part of the local orbital while a spherical harmonic describes the angular behavior.

$$\theta_{l, j_n}(r) = \sum_i C_j^{nl} N_{ij} r^{\frac{n}{2} - \frac{1}{2} l} (3.22)$$

We usually take the N_{ij} and $\frac{1}{2} l$ from Pagus et al () where optimized basis sets have been computed for the atomic or ionic system appropriate to the solid in question. In many cases, we will change this basis set to achieve localization, considering at the same time the total energy of the subsystem.

The expansion coefficient C_j^{nl} is solved by the matrix method of Koothan ().

Equation 3.21 is solved repeatedly until the self-consistency is below some predetermined value, normally one part in 10^{-6} for the charge density.

We have only used the long-range part of the external potential as the localizing potential. So, for ionic substances, the electrostatic potential will be screened while the short-range effects of the inner shells will change the local orbitals. Some anions will not localize in this situation since it is the Madelung part of the potential that stabilizes them. Since A is essentially arbitrary, we are free to alter it in whatever way that achieves optimal localization, and we often use $-j_s^2 V'_s j_s$ in equation 3.21 instead of $\tau j_s V'_s j_s$.

CHAPTER 2

Energy Band Theory

The Hartree-Fock energy bands are obtained by plotting the one-electron energies derived in equation 1.16 against the crystal momentum k . Our calculations make use of the symmetries of the crystal. In the case of these calculations, it is the zinc-blende crystal structure.

Bloch's theorem requires that the wavefunctions of the solid satisfy

$$\psi_{n\vec{k}} = e^{i\vec{k}\cdot\vec{r}} \mu_{n\vec{k}}(\vec{r}) \quad (2.1)$$

where $\mu_{n\vec{k}}(\vec{r} + \vec{R}) = \mu_{n\vec{k}}(\vec{r})$

for any lattice translation vector R . The crystal momentum is again k and n is the band index. Wavefunctions that satisfy this condition are Bloch wavefunctions.

If we look at the set of R_n , we can see that there is an element of R_n that has a minimum length, corresponding to the fundamental lattice spacing. Considering this, and the fact that R_n is a group under translation, we can see that there is a maximum k when we transform into momentum space.

Therefore, there is a finite region of non-equivalent k-points - the first Brillouin zone. This may be reduced to an 'irreducible wedge' by symmetry considerations.

The solution to the Hartree-Fock equations is lengthy for crystals, and the successive approximation nature of the calculations requires that the equation be solved several times. The Hartree-Fock equation can be rewritten in terms of the Fock-Dirac density matrix():

$$\left[-\nabla^2 - 2 \sum_i \frac{Z}{|\vec{r}_i - \vec{r}|} + 2 \int \frac{\rho(x, x')}{|\vec{r} - \vec{r}'|} dx' \right] \theta_i(\vec{r}) - 2 \int \frac{\rho(x, x')}{|\vec{r} - \vec{r}'|} \theta_i(x') dx' = E_i \theta_i(\vec{r}) \quad (2.2)$$

where $\rho(x, x') = \sum_j \theta_j(x) \theta_j^*(x')$. (2.3)

If a self-consistent density matrix is available, then equation 2.2 need only be solved once to obtain the eigenvalues and eigenfunctions. Adams () and Gilbert() have shown that the density matrix (x, x') is the same for equations 2.2 and 3.21 :

$$\rho(x, x') = \sum_{i,j} \theta_i(x) \theta_j^*(x') = \sum_{i,j} \theta_i \sum_{k,l} V_{ik}^* V_{lj} \theta_j \theta_l^* \quad (2.4)$$

So we have the required density matrix, and can obtain crystal wavefunctions from the already obtained local orbitals by constructing the Fock operator and solving equation 3.21 just once. The matrix elements of V are calculated to first order in

interatomic overlap , consistent with the calculation of the local orbitals.

The Bloch functions $\theta_{\lambda\vec{k}}(\vec{r})$ are expanded in a basis set in which the basis functions have the form

$$\phi_{T_i}^k = \sum_T e^{i\vec{k} \cdot \vec{R}_T} f_{T_i}(T - \vec{R}_N) \quad (2.5)$$

This linear combination of basis functions technique is similar to the famous linear combination of atomic orbitals technique (LCAO) except for the fact that the f_{T_i} are not free-atom orbitals, but are the local orbitals obtained previously. Note, the local orbitals are occasionally enriched for the case of virtual states. The LCPAS program will not indicate basis functions appropriate for a virtual state if that virtual state is of a different angular momentum type than the occupied states; for instance, a case in which the occupied states are all s and p-like, while the first virtual state is d-like. In this case, basis states for the virtuals are added, consisting of spherical harmonics multiplied by single STO's that are chosen to have small overlap.

Since the crystal momentum k is a good quantum number, the Fock space is diagonalized into separate spaces for each reciprocal lattice vector. The integrals necessary to perform

the calculation are k -independent and need only be performed once. Multicenter integration is done by the Lowdin α -function expansion method (). One of the sites is chosen as center and all functions are expanded in terms of spherical harmonics centered on that site. The calculations are performed using the programs KLAND and KZONE written by Kunz. The output consists of energies and coefficients of the basis functions at 20 selected points of the Brillouin zone.

Correlation Corrections

As previously mentioned, Hartree-Fock theory does not give exact solutions to the true many-electron Hamiltonian. Since we are using a single determinental wavefunction, electrons are affected only by the mean field. Electrons of the same spin have some of their true pair interactions taken into account, but there is no pair correlation at all between two electrons of opposite spin. It is obvious that the Coulomb force between two electrons is independent of spin, and should keep electrons from the near neighborhood of any other electron.

We say that the motion of electrons of opposite spins is uncorrelated, and that electrons with like spins are incompletely correlated. The correlation energy is usually defined as the difference between the energy obtained from our mean-field Hartree-Fock theory and the exact non-relativistic energy of the system. This exact energy could in principle be determined by using a computational technique called configuration interaction

27

In this method, a wavefunction is used that is a linear combination of determinants. It's impractical for all but the smallest molecular and atomic systems, and is far too time-consuming to be useful in solids.

For solids in general, and specifically in the case of the II-VI compounds under discussion, we attempt to estimate the correlation correction to the Hartree-Fock calculation. The correlation correction for the one-electron eigenvalue is the error from Koopmans' theorem () and from the independent particle model.

According to Koopmans' theorem, an orbital eigenvalue is approximately the difference between the Hartree-Fock energy of the N-electron system with the level occupied and the Hartree-Fock energy of the N-1 electron system with that same level unoccupied. These Hartree-Fock excitation energies are

$$\epsilon_{\text{hf}}^0 = E_{\text{HF}}^{(N)} - E_{\text{HF}}^{(N-1)} \quad (4.1)$$

for states that are occupied in the Hartree-Fock ground state

and $\epsilon_{\text{hf}}^e = E_{\text{HF}}^{(N+1)} - E_{\text{HF}}^{(N)}$ (4.2)

for virtual states of the Hartree-Fock ground state.

When we attempt to improve the Hartree-Fock approximation, we wish to keep the general band scheme, so

$$\epsilon_{hk} = E^{(n)} - E^{(n-1)} \quad (4.3)$$

$$\epsilon_{hk'} = E^{(n+1)} - E^{(n)} \quad (4.4)$$

where the eigenvalues are the exact eigenvalues of the system.

We assume that the correlation energies are a small perturbation of the original Hartree-Fock bands, and we can then write $E^{(L)}$ as

$$E^{(L)} = E_{HF}^{(L)} + E_c^{(L)} ; \quad (4.5)$$

here, $E_c^{(L)}$ is the total correlation energy of a system with L electrons. Equations 4.3 and 4.4 may now be written as

$$e_{nk}^0 = e_{nk}^{(N)} + (E_c^{(N)} - E_c^{(N-1)}) \quad (4.6)$$

$$e_{nk'}^0 = e_{nk'}^{(N)} + (E_c^{(N)} - E_c^{(N-1)}) \quad (4.7)$$

A useful approximation, valid for nonmetals with valence band width less than the Hartree-Fock optical band gap, was developed by Pantelides et al (). They showed that equations 4.6 and 4.7 may be replaced by

$$E_{nk}^0 = E_{nk}^{(N)} + E_{nk}^{(N-1)} (h) \quad (4.8)$$

$$E_{nk'}^0 = E_{nk'}^{(N)} + E_{nk'}^{(N-1)} (e) \quad (4.9)$$

In these equations, $E_{nk'}^{(N)}$ (e) is the self-energy of an electron

that occupies the one-electron Hartree-Fock state nk' in an

N-electron system. $E_{nk}^{(N-1)}$ (h) is the total energy change in the

remaining N-1 electrons when the electron occupying the state in

question is removed. $E_{nk}^{(N-1)}$ (h) is the self-energy of a hole.

Pantelides et al () have produced some model-independent results concerning these self-energies. They find that the self-energy of holes is always positive, and therefore the valence bands from the original Hartree-Fock calculation always move up on the energy scale upon correlation. These self-energies grow as we approach the bottom of the valence bands, so on balance the valence bands are narrowed. The self-energies of the lower electrons in the conduction band are negative, so the conduction bands move down. The models used have only small change in the amount of shift for the low-lying conduction band, and so we use a rigid downward shift for these. We end up shifting the valence bands higher and rigidly dropping the conduction bands. This produces a smaller optical gap than that obtained by the Hartree-Fock calculations.

We more nearly approach the experimental gap by this narrowing.

These self-energies were first calculated by Toyozawa (). The theory of this calculation, the electronic-polaron method, was considerably further developed by A. B. Kunz, so that it now predicts hole self-energies as well.

In the original Hartree-Fock theory particles respond only to the average position of the other electrons and ions. This is obviously incorrect, or at least incomplete; the independent charge will polarize its surroundings, especially if those surroundings have sufficient time to respond. The electronic-polaron model dresses the conduction band electrons and valence band holes with quanta of the polarization field. These quanta are excitons. In the model we are using, the excited states of the crystal are simulated by a dispersionless band of excitons. $E_{nk}^{(N)}$ and $E_{nk}^{(N-1)}$ and (e) (h) are the interaction energies of a bare electron and hole with this field. These energies are called polarization energies. This model uses second-order perturbation theory to calculate the self-energies.

These polarization energies are calculated on the basis of a model in which the hole or electron is fixed in space. This method, the Mott-Littleton method, uses a perturbative approach to find the induced dipole moments on all ions of the crystal due to the localized charges. This calculation takes into account the field from the induced dipoles - it is self-consistent. Since it takes a finite time for the crystal to respond to such a change, moving charges should induce less polarization than the model static charge. Therefore, this calculation should give an upper bound for the polarization energies of actual, mobile electrons and holes.

This electronic-polaron model is basically a long-range scheme. Only in the limit of large distance can we find these changes by assuming that they can be described by dipoles. For short distances, the shape of the wavefunctions plays a major role, and quadrupole and higher multipole effects cannot be ignored. The changes in the central atom and its near neighbors certainly cannot be modeled by a dipole very successfully!

Short-range correlation calculates the change of the nearby orbitals when an electron is added or removed. To find these corrections, we do simple atomic calculations of different ionization states, supplemented by cluster calculations in the case of negative ions where the added electron extends over a significant region of space. In the limit of zero overlap between atoms, the short range correlation correction to the hole energy is

$$E^{sr}(h) = -\frac{\mathcal{E} - E_{scf}}{E_{scf}} \quad (4.10)$$

where \mathcal{E} is the energy of the level the electron was removed from and E_{scf} is the Hartree-Fock ionization energy. The ionization energy is the difference between the Hartree-Fock energy of the system with the level occupied and the Hartree-Fock energy with that same level full. The short-range energies so calculated are again upper bounds, since electrons and holes are not as localized as this model portrays them.

The Hartree-Fock calculation and the following correlation corrections give a set of one-electron energy bands. They must now be compared to experiment to test the adequacy of our approximation.

CADMIUM SULFIDE

At room temperature and standard pressure CdS crystallizes in the zinc-blende lattice with a lattice constant of 5.818 angstroms (10.99 atomic units) and in the hexagonal form with lattice constants of 4.1348 and 6.7234 angstroms (7.3136 and 12.7054 atomic units). The zinc-blende form, the subject of these calculations, is composed of two interpenetrating face-centered cubic sublattices occupied by Cd^{++} and $\text{S}^{- -}$ ions, displaced relative to each other by $1/4$ of the diagonal of the unit cube. The symmetry properties of the zinc-blende lattice (² space group T_d) have been discussed by Parmenter (), and in the following discussions of the band structure, and notation of Pouchaert, Smoluchowski and Wigner () will be used.

We first examine the energy states at the Prillouin zone center, the Γ point. Cadmium ions contribute a filled (4d)¹⁰ shell to the valence energy region, and sulfur ions contribute a (3s)² (3p)⁶ configuration. The p and d levels hybridize to some extent, since they are separated by less than nine ev; still, the valence bands are not strongly hybridized. The top valence band is predominantly p-like (over 75%) and the next lower band is predominantly d-type, again over 75%. We expect the lowest conduction band to be derived from the cadmium 5s levels, as is usual in compounds that have any ionic character. In the zinc-blende structure, the crystal field splits the fivefold degenerate d levels into a triply degenerate state and a doubly degenerate state. The threefold degenerate p states stay degenerate under this crystal field and transform like $12\ 15$. The zinc-blende lattice has no inversion symmetry, so the bands at the gamma point need not have a definite parity. The conduction band contains both p and d contributions, in fact.

Several previous calculations have been done. The valence bands, especially the upper ones, and the lower conduction bands

have been well-described by various pseudopotential calculations. That is, they accord with current experiment. However, since the pseudopotential method is basically a parametrization scheme, in which the parameters are determined by experiment, little critical new information can be obtained. If the experimental evidence has been misunderstood or misinterpreted, the pseudopotential will simply predict the mistakes or misunderstandings that it sprang from. A pseudopotential calculation is an aid to understanding, but it tends to not be falsifiable. Such calculations, such as those by Cohen and Bergstresser () also depend on the validity of the cancellation theorem, which is not exact and which is much less valuable for systems that have localized states that are closely comparable in energy with the valence states - here, the cadmium d states are the ones not easily described because of their local nature.

A related but more theoretically rigorous technique, the orthogonalized plane wave method, has some of the same errors. In this method, the valence and conduction states are described by plane waves orthogonalized to the core states, taken as constant.

In these previous OFW calculations, as performed by Euwema and Stukel (), Euwema and Collins et al () and by Stukel et al () there have been errors of up to three ev in the p-like valence and conduction bands in compounds made of first-row atoms. Also, the 4d states are misplaced by about a rydberg - probably related to their core-like nature. The level ordering of the cadmium 4d and the sulfur s bands seems to be reversed from that measured by photoemission by about 6 ev. Altogether it is easy to see that there is a need for a first-principles calculation that correctly predicts the major features of the band structures of these materials.

Therefore, the first all-electron, self-consistent nonempirical band calculation using nonlocal exchange has been performed on CdS. The methods of calculation are as discussed earlier in this work. It should be mentioned that a self-consistent band calculation has been performed by Zunger and Freeman () using a local density approximation for the exchange potential. Their results, as well as earlier ones, will be discussed in the ensuing pages.

TABLE 4.1

STC BASIS FUNCTIONS FOR CADMIUM AND LOCAL CRITICAL COEFFICIENTS

s Basis			p Basis			d Basis	
j	n _{0j}	z _{0j}	n _{1j}	z _{1j}	n _{2j}	z _{2j}	
1	1	70.66	3	31.29	3	20.99	
2	1	45.69	2	19.62	3	11.48	
3	2	38.00	3	10.48	3	7.67	
4	2	20.71	3	6.83	4	5.75	
5	3	18.45	4	7.00	4	2.50	
6	3	10.05	4	4.55	5	2.00	
7	4	5.31	5	2.90			
8	5	2.90	5	2.00			
9	5	1.90					
j	c _{10j}	c _{20j}	c _{30j}	c _{40j}	c _{50j}	c _{21j}	
1	0.04336	-.01447	0.03145	0.03871	0.00337	-.17167	
2	0.96176	0.37037	-.00309	-.01190	-.00465	-.86037	
3	-.03876	0.17749	0.41231	0.19171	0.03936	0.10571	
4	0.01958	-1.17856	-1.21196	-.54694	-.10767	-.23043	
5	-.00903	-.02784	0.72937	0.35572	0.07401	0.17254	
6	0.00142	-.00827	0.93450	0.53579	0.08914	-.02815	
7	-.00065	0.00355	-.16742	-1.21004	-.22539	0.00925	
8	0.00033	..00172	0.00351	-.03467	0.04950	-.00394	
9	-.00018	0.00093	-.04519	-.00954	0.95921		
j	c _{31j}	c _{41j}	c _{51j}	c _{32j}	c _{42j}		
1	-.05253	0.01812	0.00473	0.08700	-.03349		
2	-.46798	0.19690	0.01288	0.66066	-.16153		
3	1.21841	-.52362	0.05304	0.30001	-.23294		
4	-.30972	-.16943	-.37952	0.01590	0.65240		
5	0.30198	0.43795	0.44531	-.00499	0.73322		
6	-.05148	0.78804	-.12748	0.00302	-.15556		
7	0.01794	0.08963	0.33543				
8	-.00775	-.01566	-.72410				

TABLE 4/.2

STO BASIS FUNCTIONS FOR SULFUR AND LOCAL ORBITAL COEFFICIENTS

	s Basis		p Basis			
j	n _{0j}	z _{0j}	n _{1j}	z _{1j}		
1	1	17.60	2	18.00		
2	2	15.45	2	13.42		
3	3	9.68	2	10.00		
4	2	5.36	2	7.75		
5	3	2.59	2	4.80		
6	3	1.63	3	2.32		
7			3	1.32		
j	c ₁₀ j	c ₂₀ j	c ₃₀ j	c ₄₀ j	c ₂₁ j	c ₃₁ j
1	0.84228	-.23268	0.06270	0.02395	0.00040	-.04392
2	0.15755	-.11309	0.03977	0.02431	0.02995	0.23470
3	-.00028	0.13620	-.02453	0.10591	0.00133	-.53346
4	0.00235	0.93730	-.33199	-.30526	0.33921	0.57490
5	-.00054	0.00402	0.51001	0.71224	0.66921	-.06509
6	0.00026	-.00035	0.59220	-.62170	0.00595	-.19300
7					-.00074	-.84226
j	c ₄₁ j	c ₃₂ j				
1	0.01330	0.00				
2	-.22359	0.00				
3	0.54462	0.00				
4	-.50114	0.00				
5	0.27387	1.00				
6	-.45037					
7	0.34676					

Polarizabilities ... and by Tessman et al () were then used for
 Cd^{++} and S^{--} along with the ... dielectric constant of 6.32

to calculate the polarization energies using the Mott-Littleton

method. We obtained values of 0.1866 ry and 0.2584 ry were

obtained as the polarization energies associated with the S^{--}

Cd^{++} holes respectively. Being less tightly bound, the sulfur anions polarize to a greater extent around a hole at the

Cd^{++} cation site than do cadmium ions around a sulfur hole,

producing a larger polarization energy for the cation. We also

calculated short-range relaxation energies for the states of

interest in the valence region; these are $E^{\text{sr}}(\text{S}^{--})_{3p} = 0.07824$ ry,

$E^{\text{sr}}(\text{S}^{--})_{3s} = 0.06302$ ry, and $E^{\text{sr}}(\text{Cd}^{++})_{4s} = 0.116$ ry. These corrections

were added to the Hamiltonian matrix which was then rediagonalized

to give the correlated valence bands. Conduction bands were

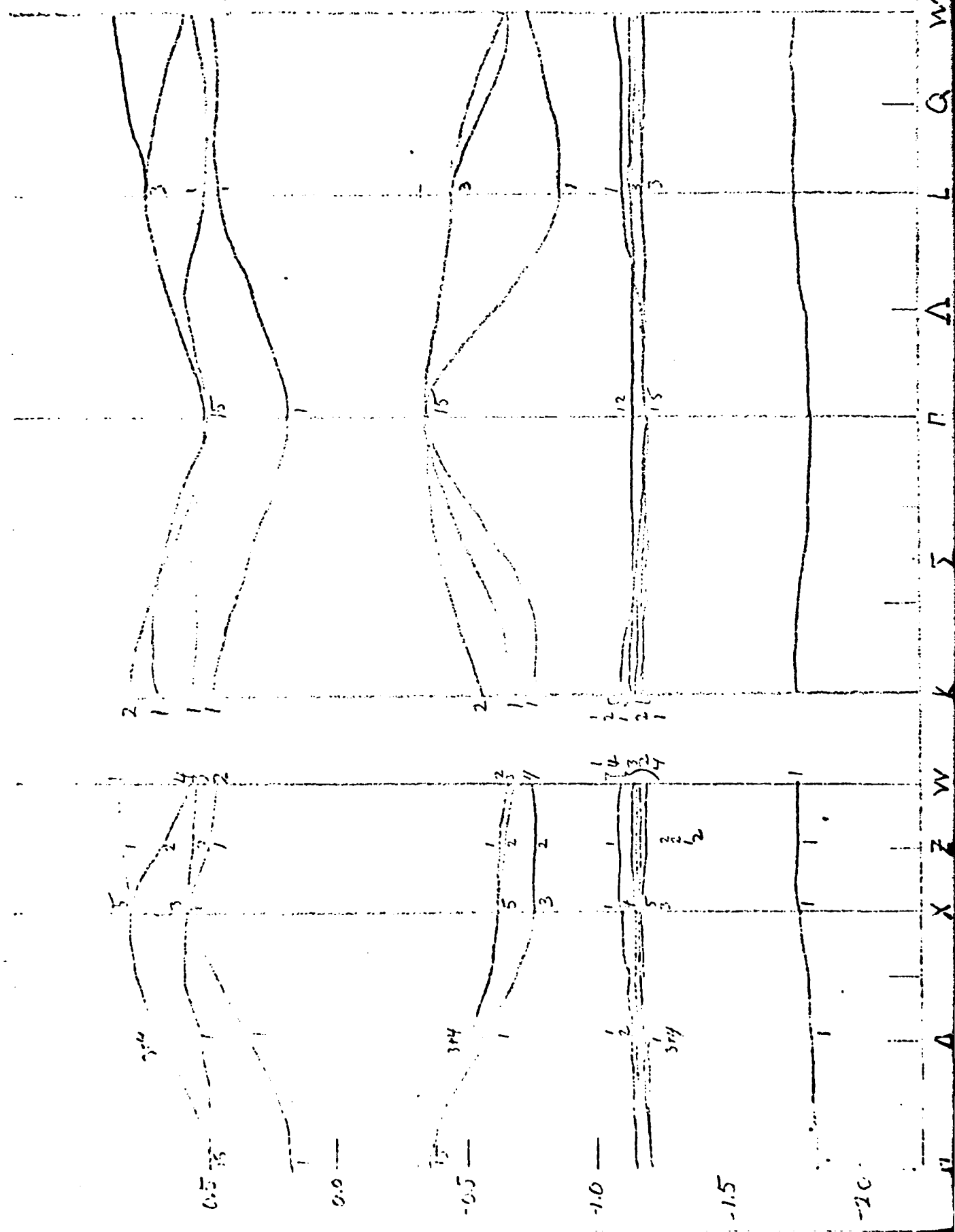
computed by shifting the Hartree-Fock conduction bands by -.2584 ry.

the polarization energy of a conduction band electron on a

Cd^{++} site.

Shown in figure 4.1 are the correlated energy bands of CdS. The calculated band structure shows cadmium sulfide to be

Figure 4.1 Correlated energy bands of CdS for the normal
lattice constant of 5.181 angstroms (10.994 au).



a direct band gap semiconductor with the gap at the gamma point.

This conclusion is in agreement with the previous band calculations.

Three major non-overlapping regions constitute the valence bands

in this system. The S⁻⁻ 3s derived band lies 19 eV below the

valence band edge and is about 1.4 eV wide. The next region

is primarily derived from the Cd⁺⁺ 4d, and lies 12 eV below the

top of the valence band. This band is about one eV wide. The

uppermost valence band is primarily derived from S⁻⁻ 3p levels,

and is about 3.9 eV wide. The lowest conduction band is s-like

and is derived from the Cd⁺⁺ 5s, S⁻⁻ 3s and S⁻⁻ 4s levels.

The band gap is found to be direct and equal to 7.1 eV.

The optical value of the gap, E_g = 2.55 eV (), obtained from

experiment, is in serious disagreement. The correlation model

here used, the electronic-polaron model and its limit,

Mott-Littleton theory, is adapted to insulators and ignores

short-range polarization effects. Such effects should be small

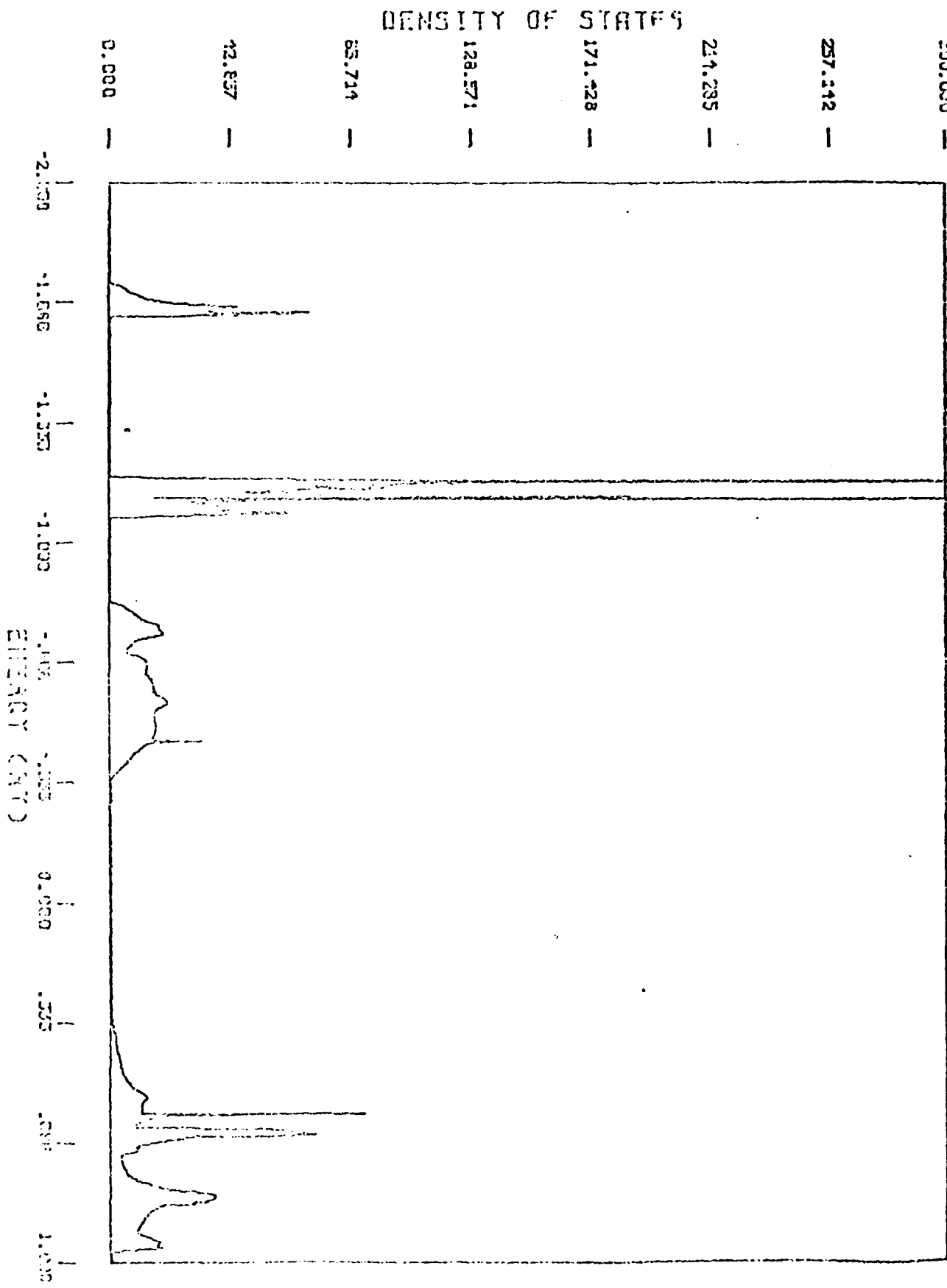
in atoms and in systems where the local orbitals are only slightly

perturbed from the free atom or ion, but in polar semiconductors

such as CdS, there is no guarantee that the local orbitals are

Figure 4.2 Density of states of CdS

CROMIUM SULFIDE DENSITY OF STATES



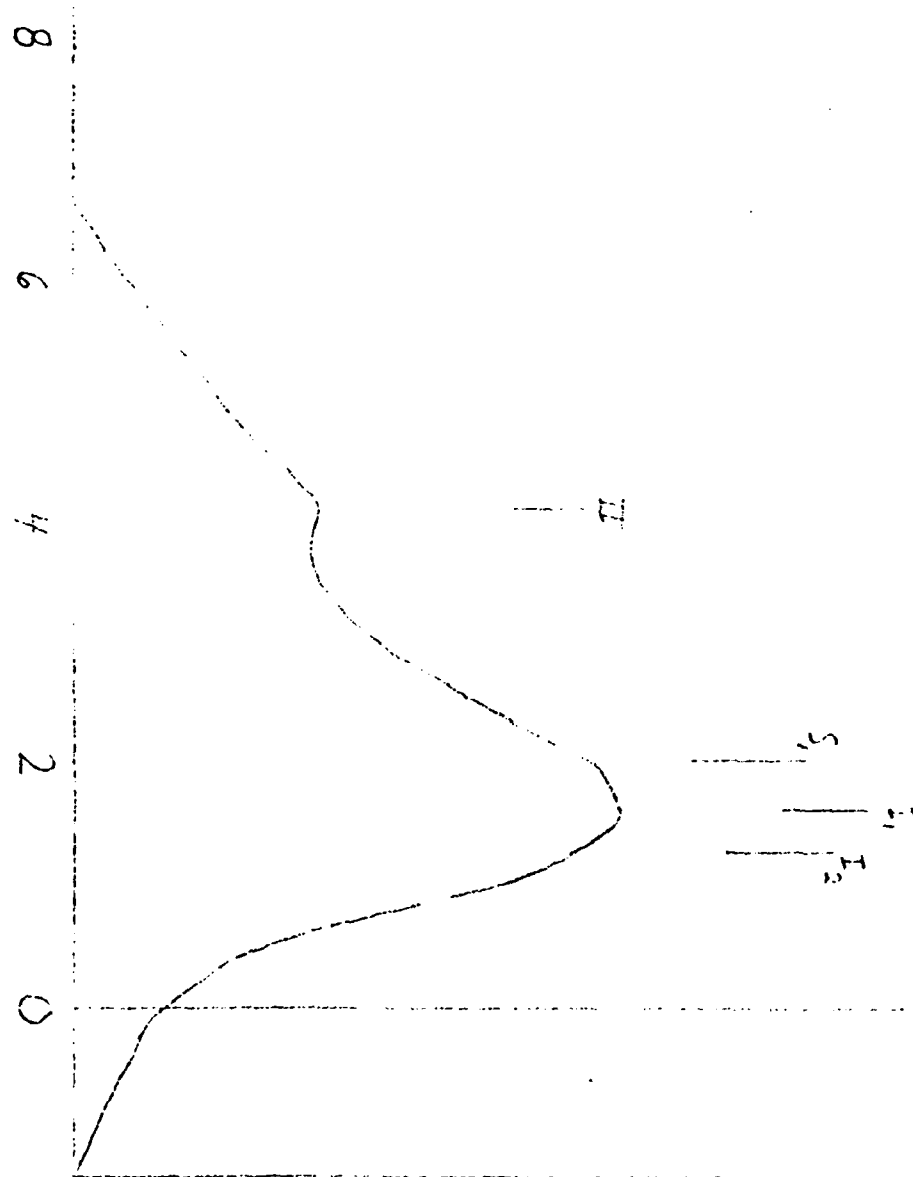
45

Figure 4.3 XPS spectrum for CdS according to Ley et al ().

I₁ and I₂ describe fine structure of the highest valence-band

peak. S₁ is a shoulder on the high-binding side of this peak.

II represents the second valence-band peak.



4

that similar to the free ions. In this class of compounds, there is substantial charge density in the internuclear region.

It has been argued that such effects act to narrow the band gap.

The density of states for CdS as calculated from the original band structure calculation is given in figure 4.2. For comparison, figure 4.3 shows the corrected XPS spectrum obtained by Ley et al (). The experimental evidence clearly shows the two peaks in the density of states of the upper valence band. The positions of these peaks are also in reasonable agreement with experiment. The upper peak lies 1.6 eV below the top of the valence band by Ley's measurements, while our calculation gives a peak at approximately 1.4 eV. Experimentally, the second peak is at 4.1 eV, while this calculation has a peak at 5.4 eV. It also seems possible to identify the shoulder of the upper peak. From our band calculation, this shoulder seems to be at about 2.6 eV, while Ley's measurements put it at 2.1 eV.

The position of the d-like levels is also correctly predicted in these calculations. These levels, primarily formed from cadmium 4d states, are found to peak at 9.6^b eV below the top of the valence band experimentally, according to Ley.

Figure 4.4 Joint density of states of CdS

CHROMIUM SULFIDE JOINT DENSITY OF STATES

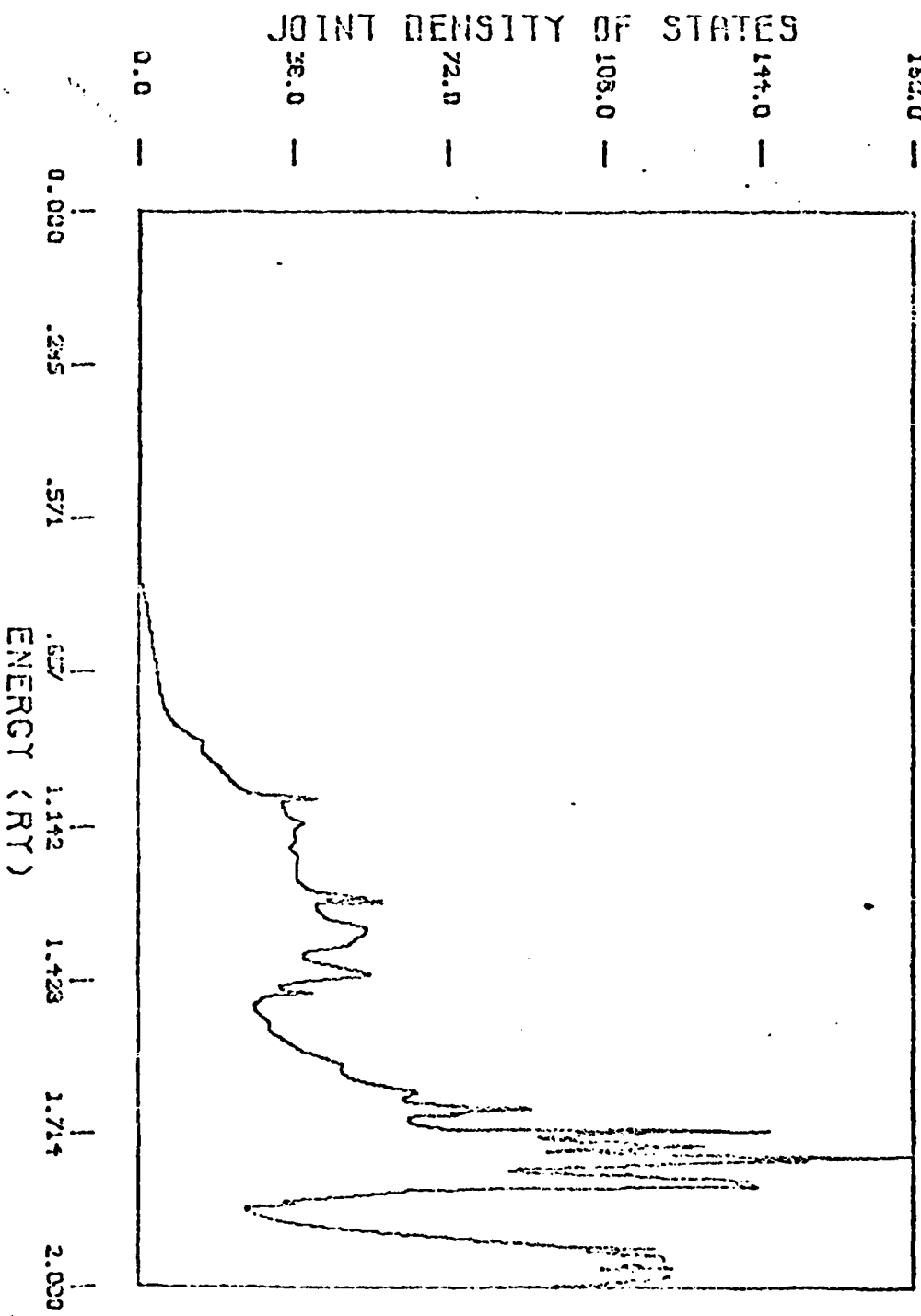


Figure 4.5 Imaginary part of the dielectric constant of CdS
(this calculation)

cas

IM. PART DIELECTRIC CONS.

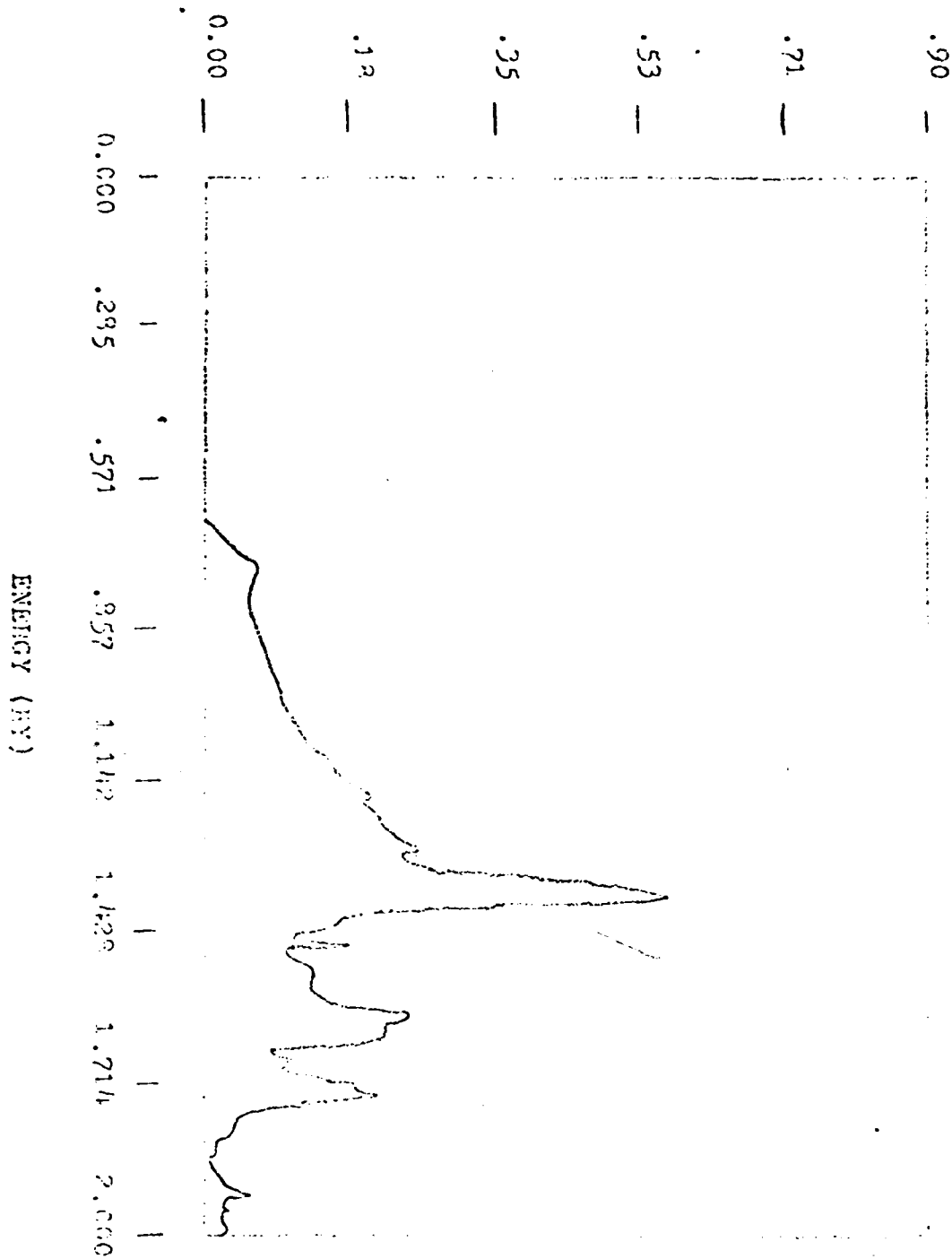
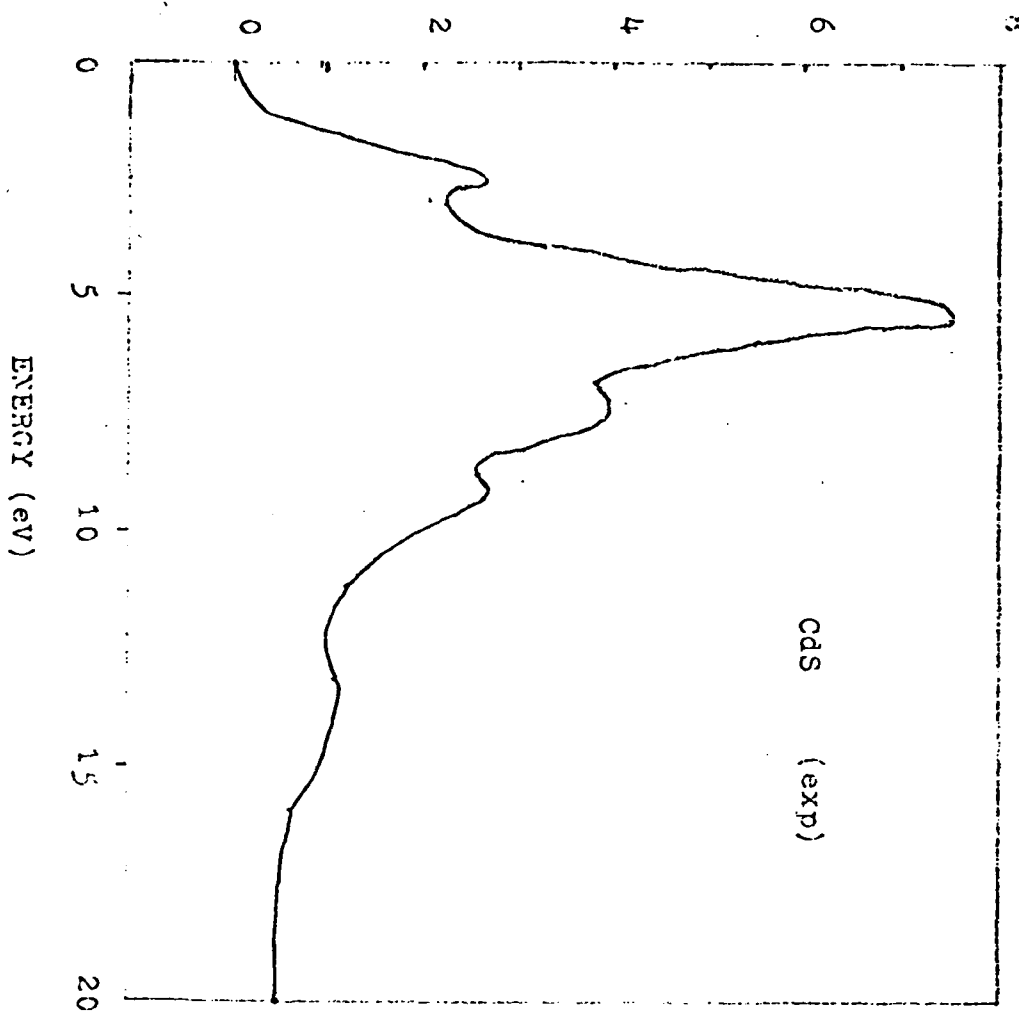


Figure 4.6 Experimentally derived imaginary part of dielectric constant in CdS, from Cardona et al ().

Derived from ultraviolet reflection measurements.

IM. PART DIELECTRIC CONS.



Our calculation gives a value of 10.3 eV below the top of the valence band, in very good agreement with experiment. This is in sharp contrast with previous pseudopotential and OFW calculations, which misplaced this band as much as 12 eV below its actual position. It should be mentioned that Ley's photoemission studies were done on CdS in the hexagonal form, but since the first two shells around the central atom are identical in the hexagonal and zinc-blende structure, the atom is exposed to a very similar potential, and no substantial change in the density of states is expected.

In figure 4.4 the joint density of states as calculated from our band structure is shown. In figure 4.5, the imaginary part of the dielectric function is calculated from the same theoretical band structure. In figure 4.6, Cardona et al extract the imaginary part of the dielectric constant from ultraviolet reflection measurements on zinc-blende CdS (). There is clear qualitative agreement, especially with the central peak and the two sub-peaks approximately 3 and 5 eV above that central peak. The tail below the central peak in energy is exaggerated due to the overestimate of the band gap in our calculations.

To sum up: these calculations correctly predict the major features of the energy bands in CdS, as determined from optical and other measurements. Insofar, this first all-electron, self-consistent non-empirical method has succeeded. The d-like levels are correctly predicted, as was not the case with earlier calculations. Nothing in the pure bulk energy bands suggests an explanation of the anomalous diamagnetism, and it would seem that the effect is not an intrinsic one. It may be hoped that this better understanding of the electronic structure of the pure solid will aid in the understanding of the anomalous diamagnetic state, perhaps by acting as necessary first step in the examination of the properties of defects and impurities in cadmium sulfide.

ZINC OXIDE

At room temperature and standard pressure ZnO crystallizes in the hexagonal (wurtzite) form with lattice constants of 3.249 angstroms (6.480 atomic units) and 5.193 angstroms (9.824 atomic units). The zinc-blende form with identical nearest-neighbor distance has a lattice constant of 4.595 angstroms (8.684 atomic units) and is the subject of these calculations. It is composed of two interpenetrating face-centered cubic sublattices occupied by Zn^{++} and O^{-} ions, displaced relative to each other by $1/4$ of the diagonal of the unit cube.

We begin again by examining the energy states at the Brillouin zone center. Zinc ions contribute a filled (3d)¹⁰ shell to the valence energy region, and oxygen ions contribute a (2s)² (2p)⁶ configuration. In this crystal structure, the threefold degenerate p states stay degenerate and transform like'.
15

The crystal field splits the fivefold degenerate d levels into a triply degenerate ¹⁵ state and a doubly degenerate ¹² state.

The zinc 3d levels and the oxygen 2p levels lie quite close, and this calculation shows shows all eight valence bands lying within a five ev region. The zinc-blende lattice has no inversion symmetry, so the bands at the gamma point need not have any definite parity. This calculation shows that this upper valence region exhibits strong p-d hybridization. The band lying beneath this upper valence region lies nearly 24 ev below the top of the valence band, and is primarily derived from oxygen 2s states..

In general, in ionic compounds such as ZnO we would expect the lowest conduction band to be primarily formed from the zinc 4s level. The actual calculation shows that although the zinc 4s states play a major role, oxygen 2s and 3s states actually play a larger role in this first conduction band. The next conduction band, triply degenerate at the zone center, are formed almost entirely from zinc 4p states . This is suggested merely by comparing zinc with its successor in the periodic table, gallium.

Several previous calculations have been performed on zinc oxide. Attempts using local pseudopotential theory, such as those by Rossler () and Bloom and Ortenburger () have not been entirely successful. Since the pseudopotential theory depends upon a cancellation of the strong core part of the potential by the usual requirement that the valence electrons be orthogonal to the core electrons, first-row elements would seem to be unsuitable for this approach. The point is that valence p-states for first row elements are not required to be orthogonal to any p-core states. Investigators have attempted to alleviate this problem by empirical adjustments to the pseudopotentials, but it hasn't worked well. When nonlocal pseudopotentials were used, as in the calculations of Chelikowsky (), a better agreement with experiment is achieved. Even so, much of the value of the pseudopotential approach is lost. There is not the same confidence that the pseudopotential will retain its predictive powers in different compounds, because the physical rationale is weakened. The modified and nonlocal calculations still suffer from all the original weakness of pseudopotentials: reliance on experiment.

TABLE 5.1

STO BASIS FUNCTIONS FOR ZINC AND LOCAL ORBITAL COEFFICIENTS

j	s Basis		p Basis		d Basis	
	n _{0j}	Z _{0j}	n _{1j}	Z _{1j}	n _{2j}	Z _{2j}
1	1	31.07	2	27.00	3	13.10
2	2	26.50	2	16.42	3	7.01
3	3	21.00	2	11.39	3	3.73
4	2	12.01	3	6.34	3	1.93
5	4	13.30	3	3.33		
6	3	6.24	4	2.67		
7	3	4.14				
8	4	2.30				
9	4	3.30				
10	2	9.00				
j	c _{10j}	c _{20j}	c _{30j}	c _{40j}	c _{50j}	c _{21j}
1	-.93261	-.28821	-.10870	-.00331	0.00195	0.01564
2	-.03561	-.18143	-.09532	-.01824	-.01406	0.26792
3	0.01250	0.01637	-.04519	-.04973	-.04893	0.73076
4	-.01042	1.13346	0.52380	0.13445	0.10761	0.01326
5	0.00293	-.01369	0.01456	-.03220	-.03323	-.00228
6	-.00191	-.01219	-.69944	-.67430	-.67032	0.00105
7	0.00085	0.00378	-.42738	0.43207	0.43002	
8	0.00003	0.00013	-.00474	0.29648	0.15094	
9	-.00031	-.00074	0.01893	-.33905	-.36103	
10	0.00120	0.02840	-.05712	0.36535	0.38957	
j	c _{31j}	c _{41j}	c _{32j}	c _{42j}		
1	-.00891	0.00896	0.03704	-.03803		
2	-.05590	-.06742	0.36525	0.00676		
3	-.36510	0.00324	0.51665	-.58505		
4	0.73105	-.00187	0.24958	0.81007		
5	0.49766	0.49813				
6	-.08803	-.86439				

TABLE 5.2

STO BASIS FUNCTIONS FOR OXYGEN AND LOCAL ORBITAL COEFFICIENTS

	s Basis		p Basis	
j	n _{0j}	z _{0j}	n _{1j}	z _{1j}
1	1	7.61	2	1.37
2	1	13.27	2	1.74
3	2	1.76	2	3.42
4	2	2.56	2	7.89
5	2	4.36		
6	2	5.94		
j	c _{10j}	c _{20j}	c _{30j}	c _{21j}
1	0.93793	-.17832	-.06946	1.45654
2	0.03915	-.02059	0.02320	-.77955
3	-.00027	0.69305	-.49485	0.45277
4	0.00357	0.14249	0.71512	-.00728
5	-.00030	0.49634	-.43475	0.01303
6	0.04136	-.32320	0.22209	

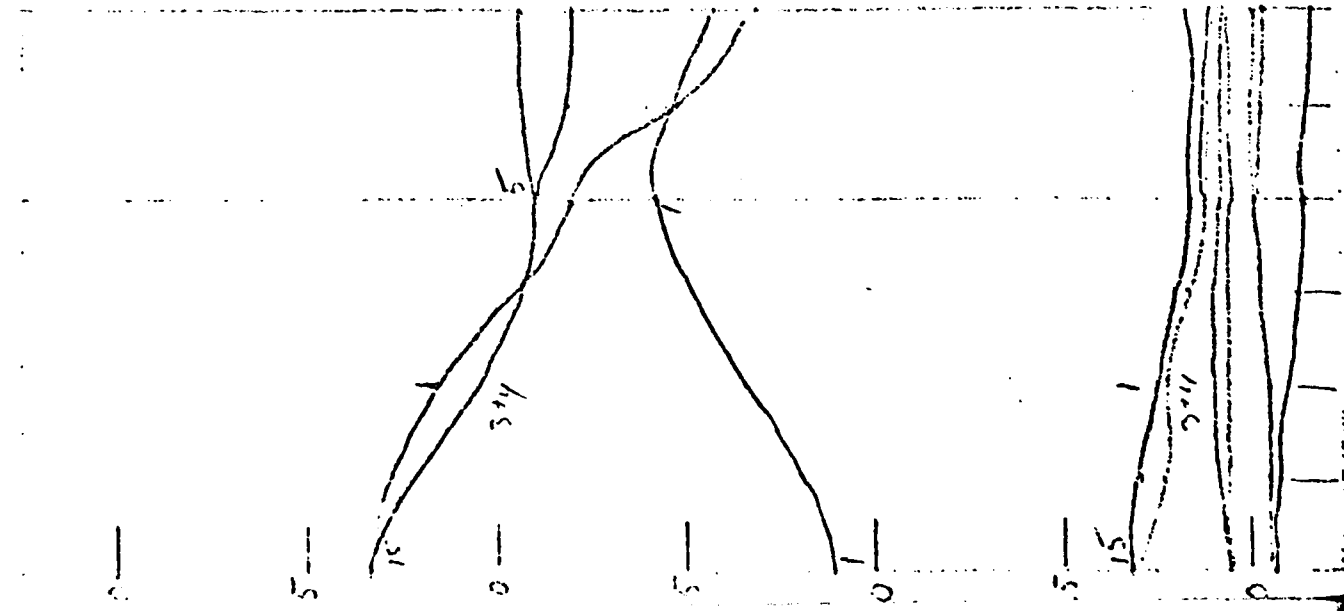
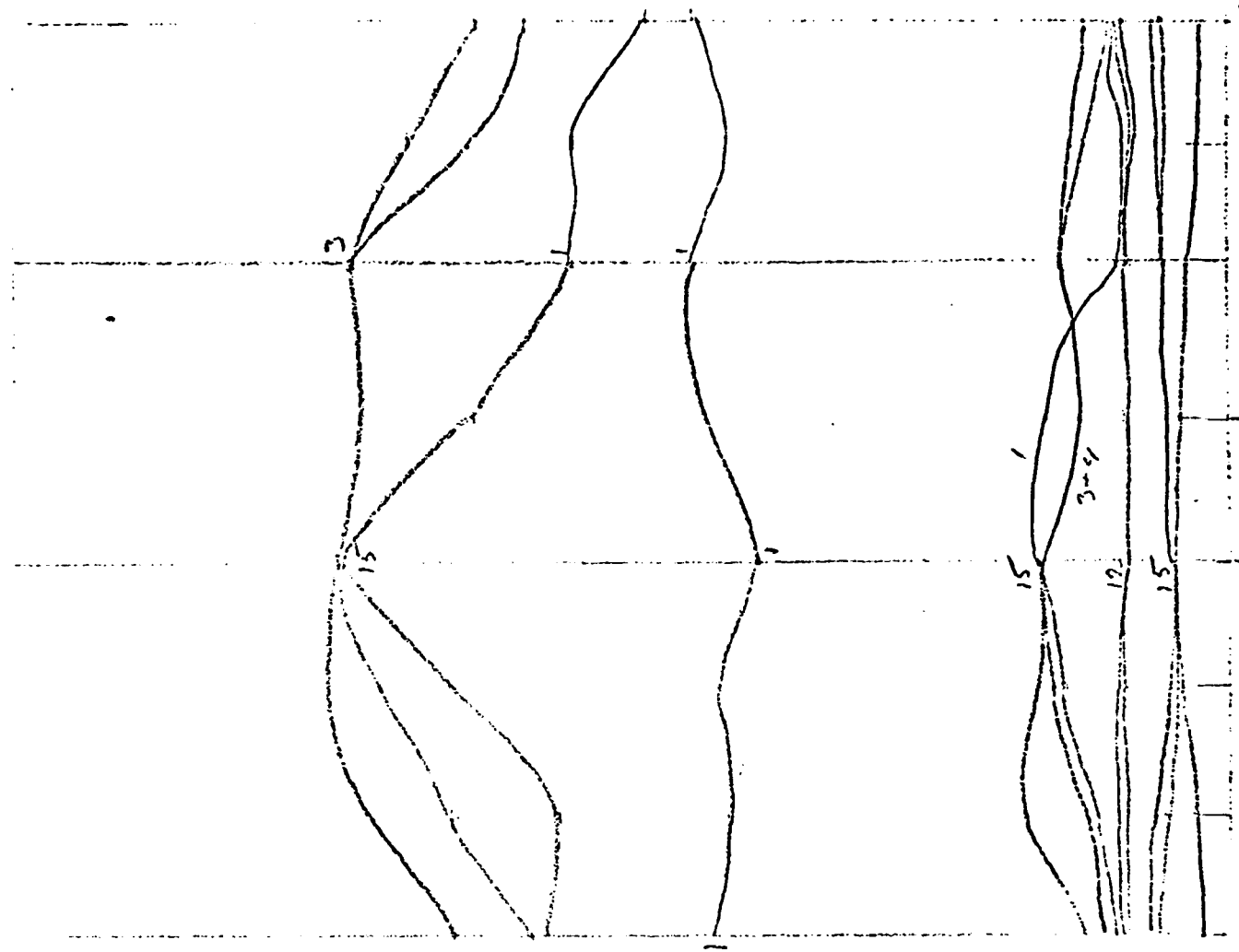
Therefore, we perform an all-electron, self-consistent nonempirical band calculation on ZnO. The methods of calculation are the same as used previously on CdS.

The calculation was begun by calculating local orbitals for zinc oxide with the normal lattice constant. The zinc and oxygen basis sets of Bagus et al () were used and were modified for this calculation. Two additional diffuse STOs were added to the s basis on zinc. The results of the local orbitals calculation are listed in tables 5.1 and 5.2 for zinc and oxygen ions, respectively.

Hartree-Fock bands were calculated for 20 k points in the irreducible wedge of the Brillouin zone. The usual exaggerated band gap appears; we proceed to apply the correlation methods previously discussed.

Polarizabilities listed by Tessman et al () were then used for Zn^{++} and $O^{- -}$ along with the optical dielectric constant of 4.036 to calculate the polarization energies using the Nott-Littleton method. We obtained values of 0.2172 ry and 0.2864 ry as the polarization energies associated with the $O^{- -}$ and Zn^{++} holes respectively. We also calculated short-range relaxation

Figure 5.1 Correlated energy bands of ZnO for the normal
lattice constant of 4.595 angstroms (8.684 au).



energies for the state of interest in the valence region: this
is $E_{3d}^{sr} (Zn^{++}) = 0.31402$ ry. These corrections were added to the
Hamiltonian matrix which was then rediagonalized to give the
correlated valence bands. Conduction bands were computed by shifting
the Hartree-Fock conduction bands by -.2864 ry, the polarization
energy of a conduction band electron on a Zn⁺⁺ site.

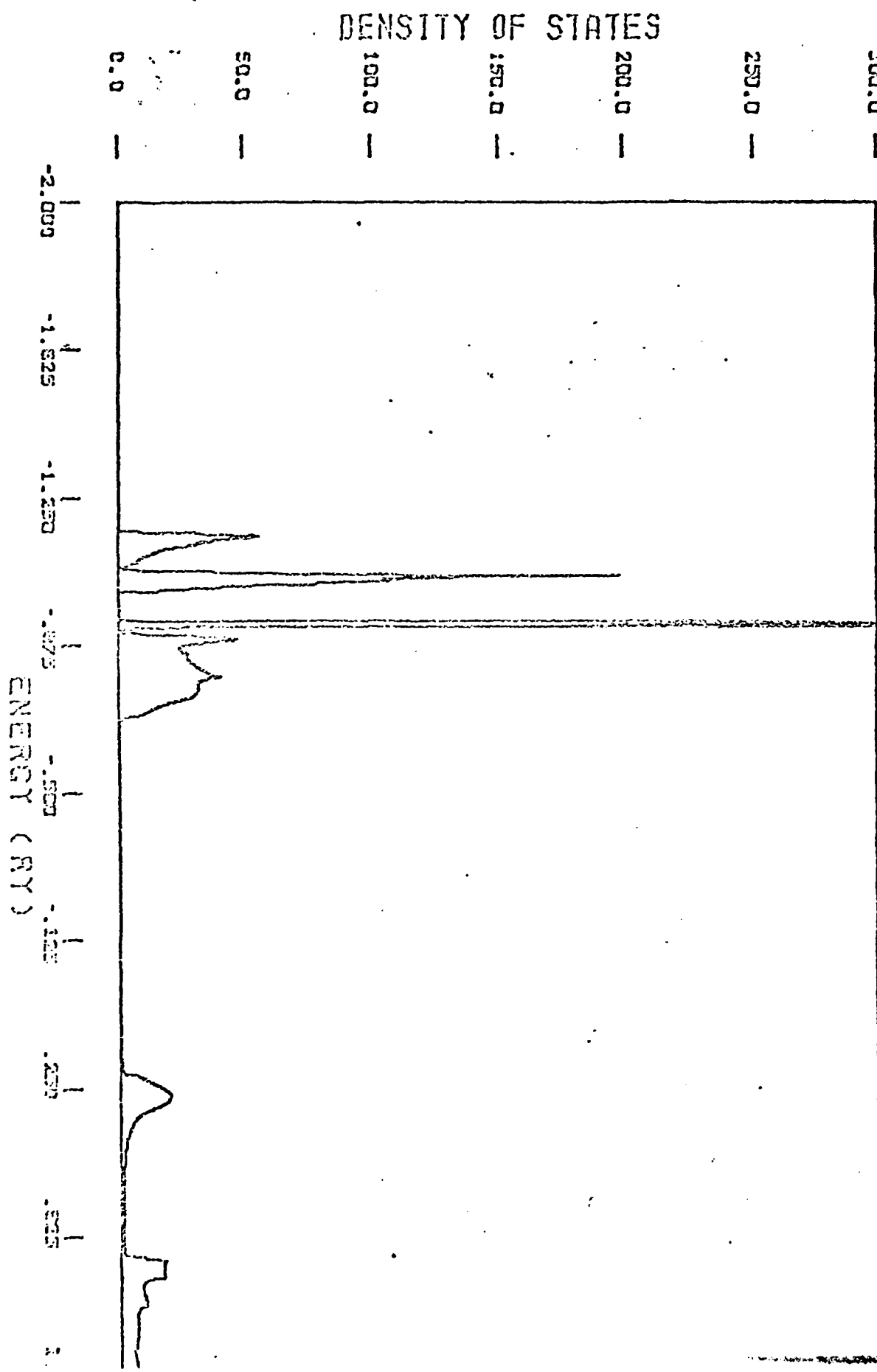
Shown in figure 5.1 are the correlated energy bands
of ZnO. The calculated band structure shows zinc oxide to be
a direct band gap semiconductor with the gap at the gamma point.
This conclusion is in agreement with previous band calculations.
Two major non-overlapping regions constitute the valence bands in
this system. The highest region is about 4 eV in width, and is
divided into two subregions with almost no overlap. The higher
and wider of these subregions is , approximately 3 eV in width,
is composed of O⁻⁻ 2p and Zn⁺⁺ 3d levels, while the lower subband
is almost dispersionless and is of almost pure Zn⁺⁺ 3d character.
The lowest valence band is about 2.3 eV in width and is composed
of O⁻⁻ 2p and Zn⁺⁺ 3d levels.

The band gap is found to be direct and equal to 10.86 eV.
Since the gap is experimentally found to be 3.3 eV, it must be

Figure 5.2 Density of states of ZnO

66

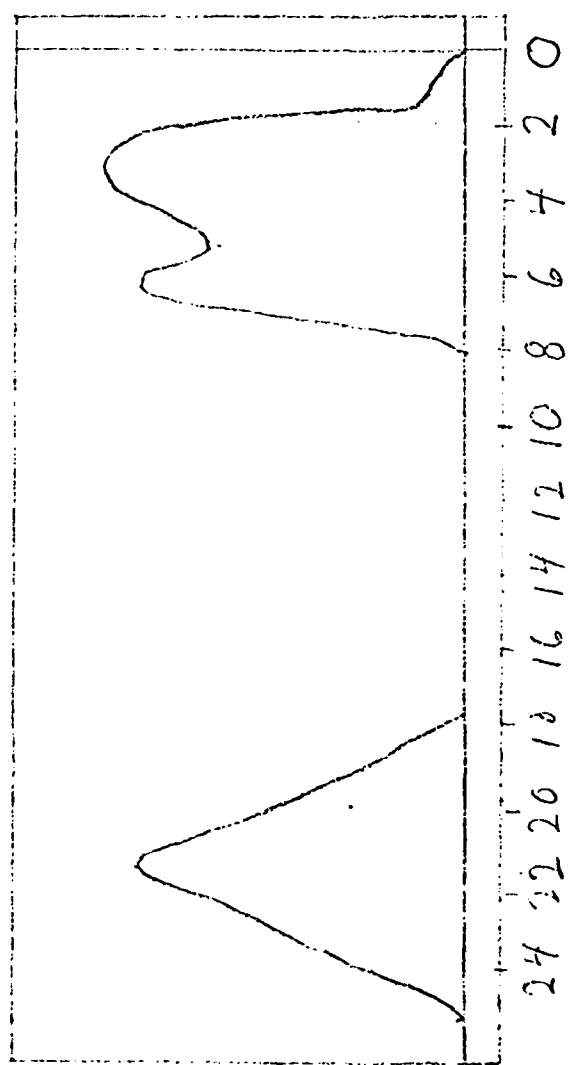
ZINC OXIDE DENSITY OF STATES



(

Figure 5.3 Corrected XPS spectrum for ZnO according to Ley et al().

68



6

that the conduction band structure here predicted is seriously in error. Previously mentioned potential problems in our correlation model may explain this discrepancy, but it seems most likely that there is some flaw in the estimate of the polarization energies.

The density of states for ZnO as calculated from our band structure is given in figure 5.2. For comparison, figure 5.3 shows the corrected experimental density of states, derived from x-ray photoemission experiments conducted by Ley et al (). The d-like levels have been subtracted out from the experimental data, since they dominate the spectra. The double peak in the density of states of the uppermost band is clearly shown in experiment and in our calculation. The d-like levels in our calculation have some structure, are not smoothed into a single peak as in the experiment. The experimental peak is centered 8.81 eV below the top of the valence band, according to Ley. Our d-complex is situated approximately 5 eV below the top, but the qualitative picture, that of a double-peaked valence band with a very sharp d-band about 3 eV below, corresponds closely with experiment.

70

Our calculations also give a band derived from O 2s states (not shown on figure 5.2) centered around 24 eV below the top of the valence band - this corresponds to the lowest peak in figure 5.3

In addition, we have calculated the joint density of states (figure 5.4) and the imaginary part of the dielectric constant (figure 5.5) for zinc oxide.

Figure 5.7 Joint Density of states of ZnO

120.0

115.0

100.0

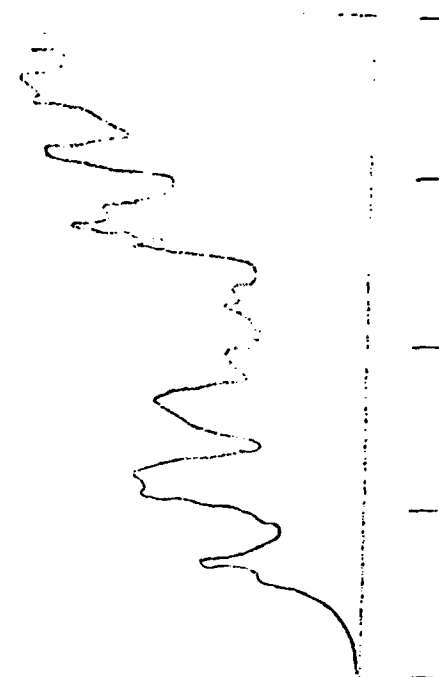
72.0

36.0

0.0

JETTY DENSITY OF STATES

ZERO JOINT DENSITY OF STATES



1
0.000 .285 .571 .857 1.142 1.428 1.714 2.000

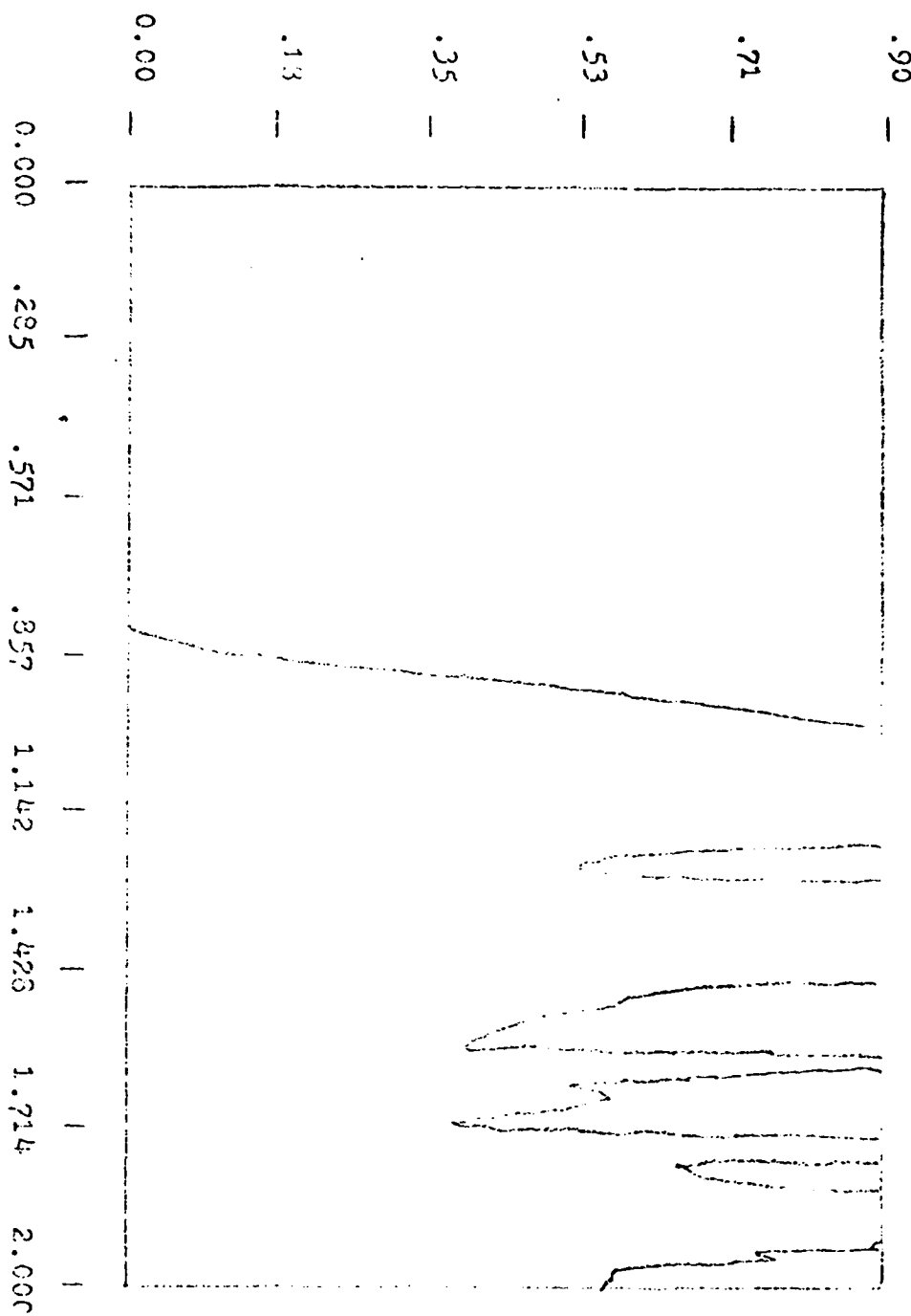
ENERGY (RY)

72

Figure 5.5 Imaginary part of the dielectric constant of ZnO

ZnO

IM. PART DIELECTRIC CONS.



ELECTRICAL

CONCLUSIONS

We've used ab initio Hartree-Fock theory, as well as relaxation and polarization correlation corrections to that theory, to calculate the electronic band structures of cadmium sulfide and zinc oxide. In the calculation of cadmium sulfide, hybridization of the Cd $5s^{++}$, S $3s^{--}$ and S $4s^{--}$ is a major factor in the lowest conduction band. The calculation shows that CdS is a direct gap semiconductor with a gap of 7.1 eV at the gamma point. This tends to show that the mechanism proposed by Abrikosov to explain the anomalous diamagnetism originally seen in CuCl (and discredited there by Weidman ()) is not applicable to CdS, since it requires a small indirect gap.

The calculated one-electron energy bands are compared with the published optical data. The valence bands are in excellent agreement with photoemission and reflection data, and, in particular

the position of the d-like band is correctly predicted, in contrast with previous calculations.

The calculation for zinc oxide shows that there is very significant mixing in the upper valence bands between the C^{--} $2p$ and Zn^{++} $3d$ levels. It seems clear that previous pseudopotential calculations that could not correctly take into account the zinc d levels were incapable of explaining the valence bands. The calculation gives a band gap of 10.86 ev, and predicts ZnO to be a direct gap semiconductor with the gap at the gamma point. In the case of both CdS and ZnO , it should be recalled that we are essentially just solving Dyson's equation, and that higher order diagrams are quite capable of accounting for the difference between the (exaggerated) gaps from our calculations and the measured experimental gaps. The fact remains that these calculations predict the valence structure; the one electron bands for zinc oxide also accord well with published optical experiments. Again, the position of the d-like bands is correctly predicted.

The anomalous diamagnetism observed in CdS remains unexplained. It seems to be an extrinsic phenomenon.

The observation of ferromagnetism upon an applied field, as well as the anomalous diamagnetism, is intriguing. It suggests that the pairing mechanism may favor a state with a spin of one, as opposed to the Cooper pair, with a net spin of zero. Each pair would have an intrinsic magnetic moment. This possibility has been discussed for classical phonon-mediated superconductivity by P. W. Anderson and P. Morel() but seems not to have been observed, except possibly at extremely low temperatures ().

An exciton-mediated pairing might well favor the $l=1$ or higher state. The superfluid state in He₃ is suggestive.

As yet the details of the interactions are not known, although it does seem that chemical impurities play a role. It may still be possible to test some of these ideas by a phenomenological theory like the Ginzburg-Landau theory. One possibility seems interesting: in the Ginzburg -Landau theory, two characteristic lengths appear, the coherence length and the penetration length. In such a model revised for a p-wave system, a third length arises, the characteristic length for the change in spin direction.

The two lengths of Ginzburg-Landau theory allow the existence of a distinctive surface, which may have a lower energy

than the bulk state, which leads to the interesting and technologically useful type II superconductors. This still exists with three characteristic lengths, but another effect becomes possible. A second surface layer is introduced; we may compare this to the earth, with crust, mantle and core. If the mantle is energetically favored, bubbles of a certain size would be energetically favored. These superconducting domains might explain the very high but finite conductivity seen in the anomalous states of CuCl and CdS, and alignment of these domains might explain the ferromagnetism seen in CdS under high applied field. At the moment, this is all speculation. We await further experiments.

(Chapter 2)

Ab Initio Energy Bands and Ionization Energies for AlP, GaP, and GaAs

J. C. Boettger and A. Barry Kunz

Department of Physics and Materials Research Laboratory
University of Illinois at Urbana-Champaign
Urbana, Illinois 61801 U.S.A.

ABSTRACT

Energy bands and ionization energies for electrons in AlP, GaP, and GaAs are obtained using a new method proposed by Kunz, et al.¹ The valence bands and ionization energies obtained are found to be in good agreement with experiment. The conduction bands vary substantially from experiment. Finally, a method for obtaining better conduction bands is proposed.

1. INTRODUCTION

A new ab initio method for obtaining correlated energy bands was recently proposed by Kunz, et al.¹ The need for a new method becomes apparent when the inherent problems associated with current ab initio methods are considered. Existing methods can be broken into two classes, those which use the nonlocal Hartree-Fock (H-F) exchange potential and those which use some local density approximation to the exchange or exchange-correlation potential. The former class of methods requires calculations which are both lengthy and complicated. Once such a H-F calculation has been performed, there is still a need to obtain correlation corrections. These corrections are poorly understood for covalent semiconductors like the III-V compounds. On the other hand, local density approximation calculations give results which are highly dependent on the choice of the exchange-correlation potential. No single potential has been found to give good results for all classes of compounds. For example, Herman, et al.², found that in using both the Slater³ and the Kohn-Sham⁴ exchange potentials for several semiconductors, the Slater potential agreed more closely with experiment for II-VI semiconductors, while Kohn-Sham exchange gave better results for the III-V compounds. Even in cases where a given potential yields the correct valence and conduction band structures, such calculations have not always been able to place the core levels in their correct locations relative to the valence bands. Finally, local density calculations have not been successful in obtaining the ionization energies for electrons in most compounds. We believe that many of these difficulties are a result of using a Hartree potential which includes a self-repulsion term, on the assumption that the potential from one electron in an infinite crystal will be negligible. As has been shown

by Kunz, et al.¹, this assumption is not correct in many cases and is a source of significant error for insulators.

The new method, which will be referred to as the Hartree-plus method, uses the correct Hartree potential, i.e. with the self-repulsion removed, along with a local exchange-correlation potential. The Hartree-plus method was applied by Kunz, et al.¹, to the solid rare gases and NaCl yielding bands which are in good agreement with both experiment and previous H-F plus correlation calculations. The III-V semiconductors provide a good test of the range of applicability for the Hartree-plus method since they are wide band semiconductors, as opposed to the rare gases and NaCl which are narrow band insulators.

In Sec.2, H-F theory is developed and correlation is discussed. The Hartree-plus theory and details of the calculations are presented in Sec.3 and Sec.4 respectively. In Sec.5, the results of Hartree-plus band calculations for AlP, GaP, and GaAs are presented and compared to experiment and previous theoretical calculations.

2. BASIC THEORY

The system of interest contains n electrons and N nuclei. Using the Born-Oppenheimer approximation⁵, and neglecting relativistic effects, the Hamiltonian is:

$$H^{(n)} = \sum_{i=1}^n f_i + \frac{1}{2} \sum_{i,j=1}^n g_{ij} \quad (1)$$

where:

$$f_i = -V_i^2 - 2 \sum_{j=1}^N \frac{Z_j}{|R_i - R_j|}$$

$$g_{ij} = \frac{Z_i Z_j}{|R_i - R_j|}$$

The energy is in Rydbergs, $e^2=2$, uppercase letters refer to nuclei, lowercase letters denote electrons, and the prime on the sum indicates that the self-repulsion term, $i=j$, is excluded. The problem now is to solve the

Schrödinger equation:

$$H^{(n)} \psi_i^{(n)}(\vec{x}_1, \dots, \vec{x}_n) = E_i^{(n)} \psi_i^{(n)}(\vec{x}_1, \dots, \vec{x}_n) \quad (2)$$

where $\psi_i^{(n)}$ is the exact n-electron wavefunction for the i^{th} excited state, and the \vec{x}_i are taken to include both space and spin coordinates.

To simplify this problem, we approximate the exact wavefunction $\psi_i^{(n)}$ with a single Slater determinant formed from a set of one-electron orbitals, $(\phi_i(\vec{x}_j))$, $i=1, \dots, n$ and $j=1, \dots, n$:

$$\psi_i^{(n)}(\vec{x}_1, \dots, \vec{x}_n) = (n!)^{-1/2} \det |\phi_i(\vec{x}_j)|$$

The expectation value of $H^{(n)}$, for the trial function $\psi_i^{(n)}$, will be a rigorous upper bound to the exact ground state energy if the resulting energy $E_i^{(n)}$ is stable against variation in the ϕ_i . Performing such a variation, subject to the constraint that the ϕ_i be orthonormal, yields an equation for the ϕ_i :

$$F\phi_i(\vec{x}_i) = \sum_j \lambda_{ij} \phi_j(\vec{x}_i)$$

where F is the Fock operator:

$$F = f_i + \int d\vec{x}_2 g_{ij} [P(\vec{x}_1, \vec{x}_2) - P(\vec{x}_1, \vec{x}_2) P(2, 1)] \quad (3)$$

$$P(\vec{x}_1, \vec{x}_2) = \sum_{j \text{ occ}} \phi_j(\vec{x}_1) \phi_j^*(\vec{x}_2)$$

$$P(2, 1) \phi_j(\vec{x}_1) = \phi_j(\vec{x}_2)$$

In eq.(3), $P(2, 1)$ is an exchange operator, the ϕ_i, ϕ_i^* may be used as operators, and $P(\vec{x}_1, \vec{x}_2)$ is the Fock-Dirac density matrix. The second term is known as the direct or Hartree term, and the last term is the exchange term. Note that the prime is no longer necessary since the Hartree self-energy is exactly cancelled by the self-exchange. Diagonalizing the matrix λ_{ij} gives the standard Hartree-Fock equation:

$$F\phi_i(\vec{x}_i) = E_i^0 \phi_i(\vec{x}_i) \quad (4)$$

The eigenvalues of eq.(4) are given meaning by Koopmans' theorem⁶.

Labelling occupied states with $i=1, \dots, n$ and virtual states with $i=n+1, \dots,$

the eigenvalues are:

$$\begin{aligned}\epsilon_i^o &= E_o^{(m)} - E_i^{(m-1)} \\ \epsilon_a^o &= E_a^{(m+1)} - E_o^{(m)}\end{aligned}\quad (5)$$

where $E_{\alpha}^{(m)}$ is the energy of the single Slater determinant approximation to the total m-electron wavefunction obtained by adding or removing the α th orbital to the n orbitals used to form the H-F ground state. Thus, ϵ_i^o and ϵ_a^o are the energies that an electron would have if its instantaneous location were independent of the instantaneous locations of the other electrons, and if no relaxation were allowed. To improve on the H-F eigenvalues while retaining the independent orbitals, one defines correlated energies by replacing the approximate energies in eq.(5) with the exact energies:

$$\begin{aligned}\epsilon_i &= E_o^{(m)} - E_i^{(m)} \\ \epsilon_a &= E_a^{(m+1)} - E_o^{(m)}\end{aligned}\quad (6)$$

The energies ϵ_i and ϵ_a are quasiparticle excitation energies. The quasiparticles associated with these energies are referred to as holes and conduction electrons respectively.

There are two basic approaches to finding the quasiparticle energies. The better understood of the two is the H-F plus correlation method, which is essentially a perturbative approach. In this method, eq.(4) is solved first, and then the correlation effects are added in as a small number of corrections. This approach to obtaining correlated bands was reviewed and developed in a formal way by Pantelides, et al.⁷ The correlation corrections are fairly well understood for both metals and narrow-band wide-gap materials. Unfortunately the III-V compounds do not fall into either of these classes. The other approach is to use an equation, analogous to the H-F equation, which somehow incorporates correlation into

the potential. This is the approach taken by the Hartree-plus method.

3. THE HARTREE-PLUS METHOD

In the past, band calculations using local exchange-correlation potentials have solved an equation of the form:

$$O_{s.p.} \phi_i(\vec{x}_i) = E'_i \phi_i(\vec{x}_i) \quad (7)$$

where:

$$O_{s.p.} = f_i + \int d\vec{x}_2 g_{12} \rho(\vec{x}_2 \vec{x}_i) + V_{xc}[\rho(\vec{r})]$$

is a single particle operator which replaces the nonlocal exchange in the Fock operator with a function, V_{xc} , of the local density, $\rho(\vec{r})$. Unlike the Fock operator, eq.(7) no longer has an exact cancellation of the self-repulsion by a self-exchange. It has generally been assumed that the self-repulsion is negligible since it comes from one electron in an infinite crystal. This is in fact true for an electron in a totally delocalized Bloch state. However, what is actually desired is the energy required to add one quasiparticle to the ground state system. For all insulators, and many semiconductors, these quasiparticle orbitals are local. In this case it is reasonable to work in the local Heitler-London representation. For such local orbitals, the self-energy is not in fact small and should be removed explicitly.

In the local representation, let $\phi_{i\mu}(\vec{r})$ be the i^{th} local orbital at site μ . The corrected potential then is:

$$H' = f_i + V_h'(\vec{r}_i) + V_{xc}[\rho(\vec{r})] \quad (8)$$

where:

$$V_h'(\vec{r}_i) = \int d\vec{x}_2 g_{12} \rho(\vec{x}_2 \vec{x}_i) - \int d\vec{r}_2 \phi_{i\mu}(\vec{r}_2) \phi_{i\mu}^\dagger(\vec{r}_2)$$

is the nonlocal Hartree potential. Although the Hartree potential is nonlocal, the nonlocality is easy to deal with by using a single Hartree potential for all orbitals of the form:

$$V_h(\vec{r}_i) = \int d\vec{x}_2 g_{12} \rho(\vec{x}_2 \vec{x}_i) - \sum_j |\psi_{j\mu}\rangle \Sigma_j^*(S.E.) \langle \phi_{j\mu}| \quad (9)$$

where:

$$\Sigma_j^*(S.E.) = 2 \langle |\phi_{j\mu}(\vec{r}_1)|^2 |\phi_{j\mu}(\vec{r}_2)|^2 |\vec{r}_2 - \vec{r}_1|^{-1} \rangle \int d\vec{r}_2 d\vec{r}_3$$

Here the bra-ket notation is used to emphasize the operator nature of the self-repulsion term.

For V_{xc} we have used the local exchange potential of Kohn-Sham⁴ and the dielectric screening function of Robinson, Bassani, Knox, and Schrieffer(RBKS)⁸. Thus:

$$V_{xc} [\rho(\vec{r})] = V_x^{ks}(\vec{r}) F^{RBKS}(\alpha) \quad (10)$$

where:

$$V_x^{ks}(\vec{r}) = -4 \left[\left(\frac{3}{2\pi} \right) \rho(\vec{r}) \right]^{1/3}$$

$$F(\alpha) = 1 - \frac{4}{3} \alpha \tan^{-1} \left(\frac{2}{\alpha} \right) + \frac{1}{2} \alpha^2 \ln \left(1 + \frac{4}{\alpha^2} \right) - \frac{1}{6} \alpha^2 \left[1 - \frac{1}{4} \alpha^2 \ln \left(1 + \frac{4}{\alpha^2} \right) \right]$$

and:

$$\alpha = .646 [\rho(\vec{r})]^{-1/6}$$

Although it might seem inconsistent not to remove the self-exchange in eq.(11), one can argue that the self-exchange will only be a significant fraction of the total exchange potential in regions of low density where $F(\alpha)$ approaches zero.

4. THE CALCULATIONS

To calculate the Hartree-plus bands shown in Figs. 1-3, we first performed an LCAO calculation using H-F atomic wavefunctions obtained by Bagus, Gilbert, and Roothaan⁹. In this calculation Nesbet's symmetry and equivalence restrictions¹⁰ were applied. Also, the crystal potential was approximated by the first term of its expansion in Y_{lm} , i.e. $l=0$. The next term in the potential would be $l=3$ and should not have a large effect on the s, p, and d orbitals, which are all that are of interest here. The potential and matrix elements are evaluated using 10 shells about the central site. We represent the remainder of the crystal by a residual

Madelung potential. To obtain this potential, we used effective charges given by Phillips¹¹. This LCAO calculation can not be expected to give good results for the conduction levels due to the use of Nesbet's restrictions¹⁰. The self-energies of the atomic orbitals have been removed for both the occupied and the unoccupied parts of the orbitals. This means that the conduction energies have been obtained as though the conduction electrons felt the potential from n-1 electrons, instead of all n valence electrons. To remedy this the self-energies are explicitly reinserted for the virtual states. At this point the Hartree-plus matrix is no longer diagonal. However the coupling between the occupied and virtual states is very weak and a second diagonalization produces new valence bands which, for GaP, differ in energy from the previous bands by at most 4%. Taking all this into consideration, we believe that the final Hartree-plus operator so obtained is consistent with the configuration used. Finally we form a Hartree-plus matrix using atomic orbitals for the core states and 89 planewaves for the conduction and valence states, and diagonalize it to obtain the final band structure. For AlP, we repeated this calculation using 27, 51, and 65 planewaves.

5. RESULTS

In all the band calculations performed here, energy levels were obtained at 21 nonequivalent points in the Brillouin zone for an f.c.c. lattice. The bands are drawn along axes of high symmetry which connect the points of high symmetry in the Brillouin zone. The symmetry labels used are consistent with Parmenter¹². In all cases the origin has been chosen to be the cation site. In addition, the orbitals and their energies are superscripted to indicate whether they are valence (v) or conduction (c) states.

The valence band structures for AlP, obtained using 27, 51, 65, and 89 planewaves, are summarized in Table 1. No experimental or theoretical values were available for comparison. The bands obtained with 89 planewaves are shown in Fig.1. By comparing the results for several numbers of planewaves, we can estimate the size of the errors due to incomplete convergence. For the top two p-derived bands, our results appear to be converged to within 0.1 eV. The third p-like band is converged to within about 0.3 eV, and the separation of the s-band and the p-bands is converged to within roughly 0.4 eV. On the otherhand, the basic structure is stable, as is the width of the s-band. We assume that this convergence information is also valid for our other calculations.

In Tables 2a and 2b, the valence band structures for GaP and GaAs shown in Figs.2 and 3 are compared to experiments and previous theoretical calculations. It is particularly interesting to compare the Hartree-plus results with the two first principles OPW calculations. For both GaP and GaAs, the Hartree-plus method gives valence band widths which are in better agreement with experiment than those obtained in the first principles OPW calculations, and are comparable in quality to the empirically adjusted calculations, especially when the lack of convergence is taken into consideration. All of the other calculations give better results than this work for the separation of the s-band from the p-bands. This error in the Hartree-plus results, 1.0 to 2.0 eV, is probably due to incomplete convergence and relaxation effects that have not been included. None of the other calculations listed give the position of the d-bands relative to the top of the valence bands. For the Hartree-plus results, we believe that the errors in the d-bands, which are less than 15%, are a result of relaxation effects, which would be expected to shift the d-bands up

relative to the top of the valence bands.

In Table 2c, the ionization energies for the cation d-levels of GaP and GaAs are compared to experimental values. This information is not given by any of the previous band calculations mentioned. The differences between theory and experiment are easily accounted for by relaxation and surface polarization effects.

In Table 3, the lowest transition energies are compared to experiment. Clearly the Hartree-plus conduction bands are in very poor agreement with experiment. To test for errors in the treatment of the self-energies, we performed a calculation for AlP with the self-energies set equal to zero. This calculation yielded conduction bands which differ from those with nonzero self-energy by no more than 0.2 eV. We therefore conclude that the errors in the conduction bands are due to the choice of the exchange-correlation potential, V_{xc} . It is not really surprising that our choice of exchange-correlation potential gives good results for the valence bands but not for the conduction bands. As was shown by Pantelides, et al.⁷, for both insulators and wide gap semiconductors, correlation effects in valence bands are a result of virtual scattering of holes, while correlation of the conduction bands comes primarily from virtual scattering of electrons. Since the mechanisms for correlation in valence and conduction bands are different, it is unreasonable to expect one exchange-correlation potential to be valid for both cases. We suggest that in future Hartree-plus calculations, it should be possible to obtain better results by using two separate potentials for the valence and conduction states.

6. CONCLUSION

Based upon the results given by Kunz, et al.¹, for the rare gases and

the results for III-V semiconductors reported here, we conclude that the Hartree-plus method should give good results for the valence bands of both insulators and semiconductors when used with the RBKS screened Kohn-Sham exchange. This method not only gives good results for the valence band widths, it also gives reasonable values for the core d levels and the ionization potentials. Based upon the calculations given, we suggest that it might be possible to find a single exchange-correlation potential that could be used to obtain good conduction bands for insulators and semiconductors in a two-potential band calculation. Such a calculation would use one potential for valence states and a second potential for conduction states. This type of calculation not only would be expected to give better Hartree-plus band structures, but would also be more consistent with what we know about correlation in semiconductors and insulators.

REFERENCES

1. A. B. Kunz, R. S. Weidman, J. C. Boettger, and G. Cochran, *Inter. J. of Quantum Chem.: Quantum Chemistry Symposium* 14, 585 (1980)
2. F. Herman, R. L. Kortum, C. D. Kuglin, and J. P. Van Dyke, *Methods in Computational Physics* (Academic, New York, 1958) 8, 193
3. J. C. Slater, *Phys. Rev.* 81, 385 (1951)
4. W. Kohn and L. J. Sham, *Phys. Rev.* 140, 1133 (1965)
5. M. Born and R. Oppenheimer, *Ann. Physik* 87, 457 (1927)
6. T. A. Koopmans, *Physica* 1, 104 (1933)
7. S. T. Pantelides, D. J. Mickish, and A. B. Kunz, *Phys. Rev. B* 10, 2602 (1974)
8. J. E. Robinson, F. Bassani, B. S. Knox, and J. R. Schrieffer, *Phys. Rev. Lett.* 9, 215 (1952)
9. P. S. Bagus, T. L. Gilbert, and C. C. J. Roothaan, *J. Chem. Phys.* 10 (1972)
10. R. K. Nesbet, *Rev. Mod. Phys.* 33, 28 (1961)
11. J. C. Phillips, *Bonds and Bands in Semiconductors*, (Acad. Press, New York and London, 1973)
12. R. H. Parmenter, *Phys. Rev.* 100, 573 (1955)
13. N. J. Shevchik, J. Tejeda, and M. Cardona, *Phys. Rev. B* 9, 2627 (1974)
14. D. E. Eastman, W. D. Grobman, J. L. Freeouf, and M. Erbudak, *Phys. Rev. B* 9, 3473 (1974)
15. L. Ley, R. A. Pollak, F. R. McFeely, S. P. Kowalczyk, and D. A. Shirley, *Phys. Rev. B* 9, 600 (1974)
16. T. C. Chiang, J. A. Knapp, M. Aono, and D. E. Eastman, *Phys. Rev. B* 21, 3513 (1980)
17. F. H. Pollak, C. W. Higginbotham, and M. Cardona, *J. Phys.*

Soc. Suppl. 21, 20 (1966)

18. M. L. Cohen and T. K. Bergstresser, Phys. Rev. 141, 789 (1966)
19. J. R. Chelikowsky and M. L. Cohen, Phys. Rev. B 14, 556 (1976)
20. V. K. Bashenov and V. I. Soloshenko, Phys. Stat. Sol. 67, K73 (1975)

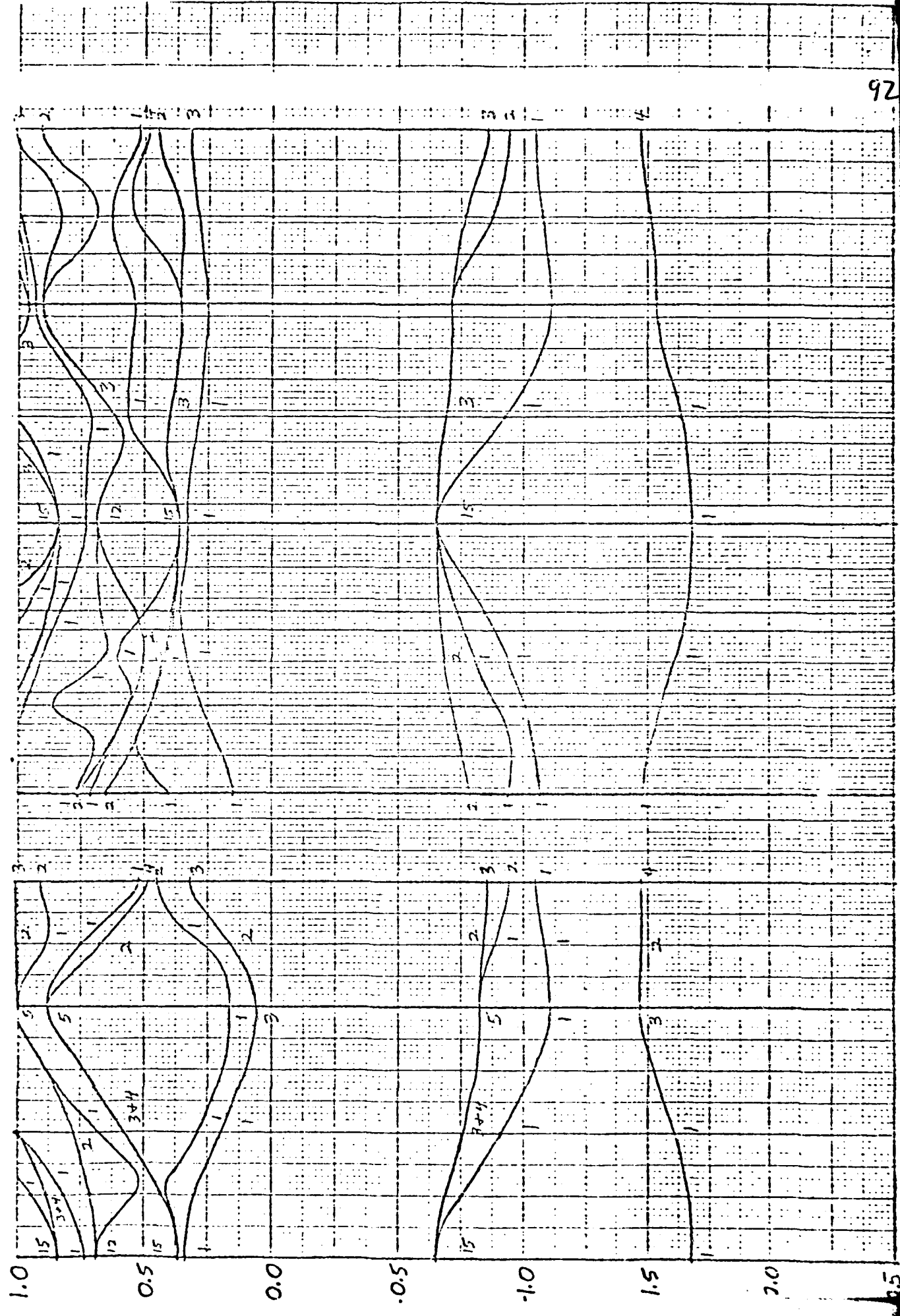
11/11/81 11:00 W 30° 10' N 101° 10' E 10.28°

5/11/81

15° E Return to 100% incl. 7 km depth

461240

Fig 1



KCS ENGINEERING DRAWING

16.12.40

Fig 2

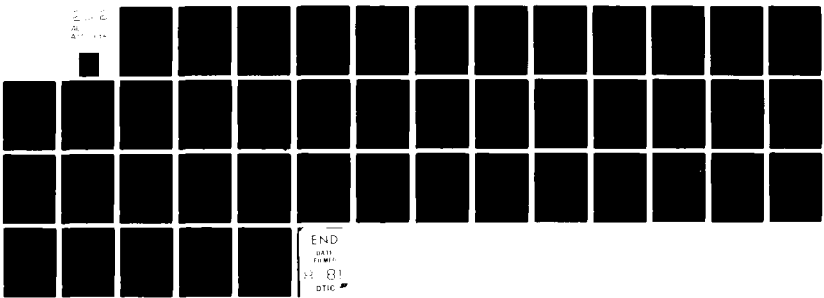


AD-A101 945 ILLINOIS UNIV AT URBANA DEPT OF PHYSICS F/G 20/12
ELECTRONIC STRUCTURE OF SOLIDS AND THEIR SURFACES AND INTERFACE--ETC(U)
JUN 81 A B KUNZ AFOSR-76-2989

UNCLASSIFIED

AFOSR-TR-81-0571

NL



END
DATA
FORMAT
R-81
DTIC

5/1/81

$\alpha = 10.6486$
AG 12M0

$K_0 \Sigma$ 20' TO THE INCHES
KODAK SAFETY FILM

Fig 3



Table 1

$\frac{E_e}{P.W.}$	27	51	65	89
L_3^v	0.51	0.87	0.81	0.78
X_5^v	2.69	2.42	2.39	2.36
W_2^v	4.27	4.20	4.04	3.96
$\Sigma_{1\min}^{(v)}$	4.77	4.28	4.14	4.06
W_1^v	6.08	5.68	5.50	5.36
L_1^v	7.17	6.54	6.30	6.17
X_1^v	6.68	6.53	6.26	6.11
X_3^v	12.21	11.64	11.31	11.12
L_1^v	13.24	12.49	12.18	11.99
Γ_1^v	15.34	14.48	14.10	13.90

Location of points in the electronic band structure of AlP relative to the top of the valence bands, $E_e^{(v)}$, in eV. Points listed for 27, 51, 65, and 89 P.W.

References for Table 2 (on next page)

- a) Photoemission with $h\nu = 16.9$ eV, Ref. 13
- b) Photoemission with $h\nu = 21.2$ eV, Ref. 13
- c) Photoemission with $h\nu = 78$ eV, Ref. 14
- d) X-ray excitation, Ref. 15
- e) Angle resolved photoemission, Ref. 16
- f) This work, Hartree-plus method
- g) Empirical $k \cdot \vec{p}$, Ref. 17
- h) Pseudopotential, Ref. 18
- i) First principles OPW with Slater exchange, Ref. 2
- j) First principles OPW with K-S exchange, Ref. 2
- k) Empirically adjusted first principles OPW with K-S exchange, Ref. 2
- l) Nonlocal empirical pseudopotential, Ref. 19

Table 2a,b,c.

Table 2a GaP

Ref. Location	Experimental					Theoretical						
	a	b	c	d	e	f	g	h	i	j	k	l
L_3^V	1.1	1.15	0.8	1.2		1.2	0.8	1.0	0.8	0.9	0.9	1.1
X_5^V	3.2	2.9		2.7		3.1	2.3	2.4	2.0	2.3	2.3	2.7
W_2^V	4.1	4.3		3.6		4.5		3.9				
$\Sigma_{1\min}^V$	5.0	5.3	4.1	4.0		4.9						
W_1^V	6.7	6.8		6.5		6.7						
L_1^V	8.0	8.5	6.9	6.9		7.2	7.4		5.6	6.0	6.0	6.8
X_1^V						7.2	7.2	7.4	5.8	6.1	6.1	7.1
X_3^V			9.7	9.5		11.7			9.5	9.4	9.3	9.5
L_1^V				10.6		12.7			10.1	10.1	10.1	10.6
Γ_1^V	18.6		11.8	13.2		14.9			11.7	11.9	11.9	13.0
Γ_{15}^V				18.6		19.8						

Table 2b GaAs

L_3^V	0.8	1.2	0.8	1.4	1.3	1.3	1.0	1.0	0.9	1.0	0.9	1.3
X_5^V	2.9	2.2		2.5	2.8	3.1	2.5	2.3	2.1	2.3	2.3	3.0
W_2^V	3.9	3.9		4.0		4.4						
$\Sigma_{1\min}^V$	4.5	4.7	4.1	4.4	4.0	4.7						
W_1^V	6.7	6.7		6.6		7.1						
L_1^V	8.0		6.9	7.1	6.7	7.3	7.5		5.7	6.1	5.8	6.8
X_1^V					6.7	7.5	7.7		6.0	6.3	5.6	6.9
X_3^V			10.0	10.7	10.75	12.0			9.9	9.7	10.5	9.8
L_1^V				12.0	11.24	13.0			10.5	10.4	11.0	10.6
Γ_1^V	18.7		12.9	13.8	13.1	14.9			11.9	12.0	12.4	12.6
$\Gamma_{15}^{(Ga-d)}$	24.4			18.8		20.4						
$\Gamma_{15}^{(As-d)}$				49.8		46.9						

Table 2c Ionization energy of the Ga 3d derived Γ_5 point

GaP	24.5				27.5							
GaAs	24.4				27.3							

2a and 2b show the location of points in the electronic band structures of GaP and GaAs respectively for this calculation, f, and also give experimental values and previous theoretical values g, h, i, j, k. A key for the references is given on the preceding page.

Table 3

Transition	AlP		GaP		GaAs	
	Exp	This work	Exp	This work	Exp	This work
Γ_1^c	3.6	13.4	2.8	12.5	1.5	11.2
L_1^c	-	12.3	2.5	11.7	2.0	10.7
X_3^c	2.4	9.7	2.3	10.1	1.9	9.4

Lowest band transitions from $\Gamma_{15}^{(0)}$, in eV, are compared with experiment for AlP, GaP, and GaAs. All experimental values are taken from Ref. 20.

Chapter 3

Surface Adsorbate Spectroscopy*

CHAPTER 1

INTRODUCTION

The electronic structure of surfaces is important in many scientific and technological fields, such as corrosion, semiconductor devices, and catalysis. However, the understanding of fundamental solid surface properties has lagged behind the progress in understanding of bulk properties. This situation has been a result of the lack of experimental methods for the quantitative characterization of the surface structure, and the theoretical complexities resulting from both the loss of symmetry at the surface and any possible reconstruction occurring at the surface. Recently developed experimental techniques such as electron energy loss spectroscopy (ELS) (), two photon picosecond spectroscopy (), surface extended x-ray absorption fine structure (EXAFS) (), and extended appearance potential fine structure (EAPFS) () have made accessible the experimental study of the structural and electronic properties of real surfaces. The

* Some support from NSF-DMR-77-2388 on this work as well

development of powerful computational methods has made possible the theoretical study of these systems.

1.1 THE INITIAL ADSORPTION OF OXYGEN ONTO THE ALUMINUM (100) SURFACE

Aluminum surfaces oxidize readily upon exposure to molecular oxygen. Several experimental studies have been performed on the initial oxidation of aluminum surfaces (). Ultraviolet photoemission spectroscopy (UPS) () and Auger spectroscopy () studies have been reported for many crystal orientations of aluminum, including the (100) surface. LEED (), EXAFS (), and EAPFS () studies have been reported.

Ultraviolet photoemission experiments () have reported a valence band resonance at 1.5 eV below the Fermi level for low oxygen exposure. This resonance is attributed to the oxygen 2p band. The shift of the aluminum 2p core level has also been measured for both low and high oxygen exposures. This shift toward lower energy is due to the dipole moment arising from the charge transfer from the aluminum substrate to the adsorbed oxygen. Work function measurements have also been reported (), with the work function found to decrease with increasing oxygen exposure. This decrease has been interpreted as being a result of incorporation of the electronegative oxygen adatoms beneath the aluminum surface.

LEED, EXAFS, and EAPFS techniques are able to probe the surface geometry of the aluminum plus oxygen adsorbate system, and thus these studies are of special interest as they will help to differentiate between various theoretical models. For low oxygen coverage, the reported Al-O bond length is 1.98 Å (), in agreement with previous theoretical calculations (). For higher exposures, a value of 1.88 Å is reported (), which corresponds to the nearest-neighbor distance in Al_2O_3 .

For theoretical studies the (100) surface is ideal: calculated electronic properties can be compared to existing Auger and UPS results, and calculated bond positions and lengths can be compared with LEED, EXAFS, and EAPFS results.

Lang and Williams (4) have studied theoretically the adsorption of oxygen onto a jellium surface. While jellium is a good approximation to bulk aluminum, it is not adequate to describe the local adsorption process. For this reason, cluster studies, which are particularly well suited to describe such local phenomena (), have been performed. Harris and Painter () and Messmer and Salahub (), have studied the adsorption of atomic oxygen onto the hole site of the Al (100) surface, reporting electronic structures which agree with existing UPS data for the initial adsorption of oxygen onto this aluminum surface. Studies of the adsorption of oxygen at the remaining two high-symmetry sites of this surface have not previously been reported. An accepted explanation of the incorporation of oxygen atoms beneath the aluminum surface does not yet exist: the calculated electronic structure and binding

potential curves for the on-top and bridge sites presented here should shed light on this problem.

In this study, the interaction between adsorbate atoms (in this case oxygen) and the aluminum (100) surface is theoretically investigated by modeling the surface with a small number of atoms and then using the unrestricted Hartree-Fock approximation to calculate the electronic structure and potential energy curves. From these potential energy curves the binding energy, bond distance, and force constants of the interaction are determined. The calculated one-electron orbitals give added insight into the chemisorption process, and calculated densities of states are compared with photoemission data. This calculational procedure is able to accurately describe the localized bonding of an adsorbate onto a surface site, the aspect of chemisorption considered most important ().

The localized nature of the chemisorptive bond is indicated by several kinds of experimental evidence. An adsorbed atom or molecule can be observed to hop from one localized site to another (). Infrared spectroscopy studies have found that the vibrational spectra of intermediates on surfaces are often very similar to the spectra of isolated molecules (). These experimental results reinforce the intuitive notion that the chemisorptive bond is similar in nature to the familiar, localized chemical bond.

In general, the loss of symmetry in the direction perpendicular to the surface leads to the choice between two drastic approximations in theoretically modeling the surface-adsorbate interaction. The maintenance of translational symmetry in the plane parallel to the surface greatly simplifies the computational difficulties and allows for the use of the powerful methods developed for bulk band structure calculations. The alternative approximation, simulating a small section of the surface by a cluster of atoms, can more effectively describe the localized interaction of the surface with a single atom.

Numerous calculations of the electronic structure of surfaces using the approximation of a semi-infinite surface have been reported (). The major drawback of this approach is that, in general, a semi-infinite monolayer of adsorbed atoms must be considered in a chemisorption calculation. This limitation is a direct result of the symmetry assumed, and therefore only qualitative calculations can treat a single adatom on a semi-infinite surface.

By relaxing the symmetry requirements of the semi-infinite surface, one gains increased flexibility and freedom. For instance, atoms can be brought down over a variety of possible bonding sites. Roughened and stepped surfaces, exposed corners, and small particles, which experimental work indicates are often sites favored for chemisorption, can easily be simulated by the cluster approach. Use of the semi-infinite surface, by contrast, is limited to studies of the perfect surface.

Once the appropriate cluster has been chosen to simulate the surface, the electronic structure of the cluster-adsorbate system must be calculated. The method used here is the unrestricted Hartree-Fock approximation, from which electronic wavefunctions, electron energy eigenfunctions, and the total electronic energy are calculated. This calculation is repeated at varying adsorbate-surface separations, and the potential energy curve can be generated from the differences in total electronic energy.

The Hartree-Fock approximation as the method of calculation is attractive due to two important advantages. The method is a convenient first step towards an ab initio solution of the many-particle Schrodinger equation for a fermion system, and gives a useful zeroth-order wavefunction for a perturbation calculation of the many-body problem. Second, it is the most advanced calculational method in which elementary physical intuition is applicable. In more complete calculations, there is no longer a one-to-one correspondence between particles and one-particle wavefunctions, and the independent particle approximation is no longer applicable.

1.2 THE ELECTRONIC PROPERTIES OF THE SILICA SURFACE

The electronic structure of crystalline silica (SiO_2) is of technological interest in, for example, the manufacture of solid state electronic devices. Consequently, there has been considerable

experimental effort in this area. In a recent review of experimental and theoretical results, Griscom () has compiled much of the existing data on the bulk properties of silica. The band gap has been found to be about 8.9 eV, with a valence band width of approximately 11 eV. Ultra-violet photo emission spectroscopy (UPS) studies by Ibach and Rowe () have detected no occupied surface states within the band gap. Williams () has studied silica surfaces grown on crystalline Si and found traps at 2 eV below the bulk silica conduction band edge. These traps act like Coulomb centers with a positive charge. It is with the silica surface and its defects that the current investigation is concerned.

Several recent experimental studies have investigated surface states of silica (). Schwidtal () has found a radiation-induced feature at 91 eV on the high-energy side of the Si L_{23} VV (V=valence) transition in the Auger electron spectrum (AES), and suggests that it is due to an Si L_{23} VD (D=defect) transition. He further suggests that this defect is the E'_s center, which is a dangling singly-occupied sp^3 orbital of silicon. Ibach and Rowe (), Fujiwara and Ogata (), Lieske and Hezel (), and Bermudez and Ritz () have measured electron energy loss spectra (ELS) and found peaks in the second derivative spectrum at about 3.5, 5.0, and 7.4 eV (Fig. 1). Ibach and Rowe have attributed these transitions to a partially oxidized surface region, SiO_x , where $1 < x < 2$. Fujiwara and Ogata () have shown the states associated with these transitions to be at the surface, and concluded they were due to metastable SiO_x . Lieske and Hezel () have associated

the final states with Si-Si bonds found in SiO_x . Most recently, Bermudez and Ritz () have studied this transition, and found the final state to be due to "a chemically stable species formed after rupture of the silica network," and attributed these properties to a surface Si=O double bond. For this bond to exist, the silica surface must undergo reconstruction. Evidence for such reconstruction from low energy electron diffraction (LEED) measurements is due to Janossy and Menyhard (). Also, Hochstrasser and Antonini () have observed what they believe to be recombination luminescence due to the rearranging of the surface Si-O bonds immediately after cleaving. They measured the lifetime of this luminescence to be less than 10^{-6} seconds.

Theoretical studies of the silica bulk electronic properties have been performed (), and the calculated densities of states are in good agreement with experiment, except for the AES peak at 91 eV and the ELS peaks at 3.3, 5.0, and 6.8 eV. Both of these discrepancies can be accounted for by allowing for the existence of islands of silicon in the bulk SiO_2 . Bennett and Roth () have calculated, using the Huckel approximation, the electronic properties of many clusters which approximate silica, and in particular gave attention to defects. These calculations were performed in the bulk; however, the clusters were sufficiently small that they can be interpreted in terms of surface defects, or in terms of a surface SiO_x region. For oxygen deficient clusters with a relaxation of the silicon atoms near the defect, the calculated energy levels showed transitions at approximately the same energy values. These are, however, probably due to small clusters (2-3

atoms) of silicon in the SiO_x . Laughlin, et al. (), using a tight binding method, have calculated similar defects and have also found states which appear in the gap, at about 5 eV above the valence band edge. They have also studied the E' center, and found a level lying just below the bulk conduction band. Pollmann and Pantelides () have performed a calculation using a Green's function formulation on the ideal terminated cubic (β -cristobalite) surface. Using an admittedly crude model for the surface, they found no states in the band gap.

The purpose of the current investigation is to study the silica surface, giving particular attention to the three ELS peaks observed at 3.5, 5, and 7 eV. The cluster model is again employed, for the same reasons given in section 1.1. Of the three models proposed by experimentalists to account for these transitions, the only one which has previously been calculated theoretically is the SiO_x model. In chapter 4 are presented calculations of the one-electron energy levels for the remaining two models, the E'_s center, and the $\text{Si}=\text{O}$ surface double bond. A comparison is then made between the three models and experiment.

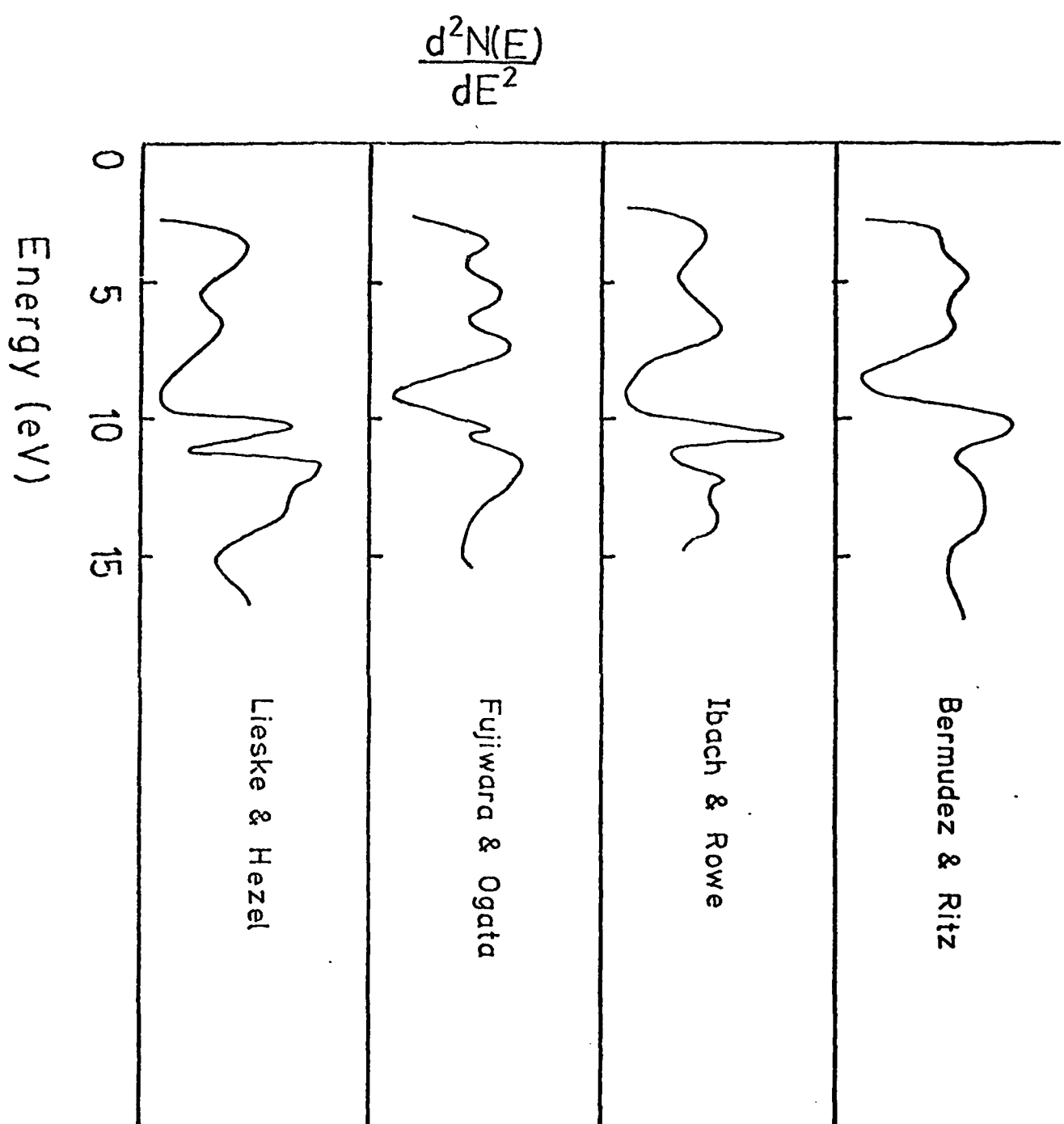


Fig 1.

METHOD OF CALCULATION

An exact solution to the wave equation for a large cluster of atoms is not at present attainable. In fact, such a solution, while nice in a mathematical sense, would be difficult to interpret physically. The ab initio Hartree-Fock theory provides an approximate method of solution to determine the electronic structure of a large cluster of atoms which is both easily handled by contemporary computers and well suited for straightforward interpretation.

2.1 HARTREE-FOCK THEORY

Ab initio Hartree-Fock theory is used to calculate the electronic wavefunctions and energies for the finite clusters studied in this work. The solids studied contain atoms of low atomic number; therefore relativistic effects are small and will be ignored. Using the

nonrelativistic Schrödinger theory, the many-body wavefunction Ψ , which is a function of electronic and nuclear space-spin coordinates, is determined by the equation

$$H \Psi(\vec{x}_1, \vec{x}_2, \dots, \vec{x}_n) = E \Psi(\vec{x}_1, \vec{x}_2, \dots, \vec{x}_n) \quad (2.1)$$

where H is the many-body Hamiltonian

$$H = H_e + H_n + H_{int} \quad (2.2)$$

with

$$H_e = - \sum_i \frac{1}{2} \nabla_i^2 + \frac{1}{2} \sum_{i \neq j} \frac{1}{|\vec{r}_i - \vec{r}_j|}$$

$$H_n = - \sum_I \frac{1}{2M_I} \nabla_I^2 + \frac{1}{2} \sum_{I \neq J} \frac{\frac{Z_I Z_J}{|\vec{R}_I - \vec{R}_J|}}{|\vec{R}_I - \vec{R}_J|} \quad (2.3)$$

$$H_{int} = - \sum_{i,I} \frac{Z_I}{|\vec{r}_i - \vec{R}_I|}$$

Here we have used atomic units, where \hbar , m_e , and $e=1$, the unit of length is the bohr ($1 \text{ bohr} \approx 0.529 \text{\AA}$), and the energy is given in Hartree ($1 \text{ Hartree} \approx 27.2 \text{ eV}$). Upper case letters refer to nuclear properties: \vec{R}_I is the position of the I^{th} nucleus, and M_I is its mass. Lower case letters refer to electronic properties: \vec{r}_i is the coordinate of the i^{th} electron. The four-vector \vec{x}_i denotes both the spatial coordinates and the spin of the i^{th} electron.

The Schrödinger equation is simplified by employing the Born-Oppenheimer approximation () to separate the nuclear and electronic coordinates. The total wavefunction is assumed to be

separable:

$$\Psi(\vec{x}, \vec{X}) = \phi(\vec{X}) \psi(\vec{x}, \vec{X}) \quad (2.4)$$

The nuclear wavefunction $\phi(\vec{X})$, is now a solution of the equation

$$\left[-\sum_I \frac{1}{2m_i} \nabla_i^2 + \epsilon(\vec{R}) \right] \phi(\vec{X}) = E \phi(\vec{X}) \quad (2.5)$$

while the electronic wavefunction, $\psi(\vec{x}, \vec{X})$, is a solution of the equation

$$\left[H_e + H_{int} \right] \psi(\vec{x}, \vec{X}) = E(\vec{r}) \psi(\vec{x}, \vec{X}) \quad (2.6)$$

A solution of this electronic Schrödinger equation depends on the nuclear coordinates \vec{R} and in turn defines a potential energy function of the coordinates:

$$\epsilon(\vec{R}) = E(\vec{r}) + \sum_{i,j} \frac{\vec{z}_i \cdot \vec{z}_j}{|\vec{r}_i - \vec{r}_j|} \quad (2.7)$$

which determines the motion of the nuclei. The problem is now reduced to solving the electronic Schrödinger equation for a particular set of nuclear coordinates. This equation cannot in general be solved exactly; one therefore takes refuge in the independent particle model for a method of obtaining an approximate solution.

This approach is mathematically equivalent to a separation of variables technique. The many-electron wavefunction, which is a functional of the space-spin coordinates of all of the electrons, is assumed to be a product of orbitals which are functions of one-electron space-spin coordinates. However, the Pauli principle requires that the many-electron wavefunction be antisymmetric under the exchange of any two electrons. Therefore, the total electronic wavefunction is approximated by an antisymmetrized product of one-electron orbitals:

$$\Psi(\vec{r}_1, \vec{r}_2, \dots, \vec{r}_n) = \frac{1}{\sqrt{n!}} \langle \hat{\Omega} \left| \phi_1(r_1) \phi_2(r_2) \cdots \phi_n(r_n) \right| \rangle \quad (2.8)$$

where $\hat{\Omega}$ is the antisymmetrizer. Since the Schrödinger equation is still not in general solvable analytically, the variational principle is introduced to obtain approximate solutions. The variational principle states that the normalized expectation value of the Hamiltonian using approximate wavefunctions is a rigorous upper bound to the exact energy. The approximate wavefunction can then be varied to minimize the energy and thereby be the best approximation to the exact wavefunction. Applying the variational principle to the electronic Schrödinger equation, and using an antisymmetrized product of one-electron orbitals, we obtain the Hartree-Fock equations:

$$F\phi_i(\vec{r}) = \sum_j \lambda_{ij} \phi_j(\vec{r}) \quad (2.9)$$

where F is the Fock operator:

$$F\phi_i(\vec{r}) = \left[-\frac{1}{2}\nabla^2 - \sum_j \frac{Z_j}{|\vec{r}_j - \vec{r}|} + \sum_j \int \frac{|\phi_j(\vec{r}')|^2}{|\vec{r} - \vec{r}'|} d\vec{r}' \right] \phi_i(\vec{r}) + \sum_j \phi_j(\vec{r}) \int \frac{\phi_j^*(\vec{r}') \phi_i(\vec{r}')}{|\vec{r} - \vec{r}'|} d\vec{r}' \quad (2.10)$$

The matrix elements λ_{ij} are Lagrange multipliers, and have been introduced to insure the orthonormality of the one-electron orbitals. In general, a unitary transformation can be performed on the orbital space which diagonalizes this matrix. The Hartree-Fock equations can then be written in the standard form:

$$F\phi_i(\vec{r}) = \varepsilon_i \phi_i(\vec{r}) \quad (2.11)$$

These integro-differential equations are normally solved via an

iterative procedure. Thus, the electron orbitals are determined in the average field of all the other electrons. The only constraints imposed on the wavefunction are that the orbitals be orthonormal and be functions of the space-spin coordinates of only one electron. This level of approximation is called generalized Hartree-Fock (GHF) and has yet to be solved, so further constraints are imposed to simplify the calculation. The simplest constraint which can be imposed is to require that the orbitals be eigenfunctions of S_z , i.e., the orbitals be of the form:

$$\psi_i(\vec{r}) = \begin{cases} \phi_{i\alpha}(\vec{r}) \alpha \\ \phi_{i\beta}(\vec{r}) \beta \end{cases} \quad (2.12)$$

where $\psi_i(r)$ is the spatial part of the orbital, and α and β are the spin-up and spin-down eigenfunctions of S_z , respectively. The form of the Hartree-Fock equations is unaffected by this constraint, and this level of approximation is known as the unrestricted Hartree-Fock (UHF). The UHF method has been used for numerous practical calculations of atoms, molecules, and solids (), and is the method used in this study.

Additional restrictions may be placed upon the one-electron orbitals in order to further simplify the calculations. The spatial parts of the orbitals may be required to be symmetry eigenfunctions of the cluster under consideration, i.e., each orbital must transform as an irreducible representation of the space group of the cluster. Finally, for doubly occupied orbitals the spin-up and spin-down spatial orbitals may be assumed to be equivalent. This level of approximation is called

the restricted Hartree-Fock method (RHF). One advantage of RHF is that the one-electron orbitals are eigenfunctions of both spatial symmetry and spin. However, for singly occupied orbitals complications arise in that the Fock operator differs for open and closed shells of the same symmetry, thus not allowing the single determinant to properly describe the wavefunction. The UHF method, while not necessarily obtaining a wavefunction which is an eigenfunction of spin and spatial symmetry, does give a lower (i.e., better) eigenfunction of energy. Since the "best" solution to equation 2.6 is the wavefunction which gives the lowest energy, the UHF method has therefore been used in this calculation.

2.2 CLUSTER MODEL

Localized phenomena in solids, such as point defects or surface adsorbates, can be modeled effectively by using a finite cluster of atoms (). Since the cluster is intended to represent a much larger system, one must apply appropriate boundary conditions for the cluster to simulate the effects of the environment. These have been discussed by Kunz and Klein (), and will be briefly reviewed here.

The solution to the Hartree-Fock equation (2.11) is sought for a finite cluster. Suppose the region of the cluster is termed A, and the remainder of the system, the environment of A, is termed E. The problem is to partition the system rigorously into a cluster and an environment. Let us consider the method of local orbitals of Adams, Gilbert, and

Kunz(). Here the Fock operator, F , of the entire system is divided into a part which includes the kinetic energy, nuclear attraction of the electrons and nuclei inside A , along with the electron-electron potential for the electrons assigned to A , F_A ; and another part which is the potential in A due to the environment, U_A :

$$F = F_A + U_A \quad (2.13)$$

It is desired to study only part of the system, so instead of the normal Hartree-Fock equation (2.11), consider instead the local orbitals equation:

$$\left[F_A + U_A - \rho W_f \right] \phi_i = \pi_i \phi_i \quad (2.14)$$

where W is an arbitrary Hermitian operator. Consider now an ionic system. The potential due to the environment, U_A , may be divided into two parts: V_A^M is an ionic (Madelung) contribution and is long range, and V_A^S is the remainder and is short range. Let $W = V_A^S$. Making use of the projector properties of P , $P\phi_i = \phi_i$, and solving for the occupied orbitals, equation (2.14) becomes

$$\left[F_A + V_A^M \right] \phi_i = \pi_i \phi_i - V_A^S \phi_i + P V_A^S \phi_i \quad (2.15)$$

Considering only the orbitals of equation (2.15) which lie in A , the solutions should penetrate only weakly into E . Because V_A^S does not appreciably penetrate A , and because $V_A^S \phi_i$ is cancelled by $V_A^S \phi_i$ in the limit of self-consistency, the approximate equation for the cluster, including the interaction with the remainder of the system, is then

$$\left[F_A + V_A^M \right] \phi_i = \pi_i \phi_i \quad (2.16)$$

This approximate equation is simply the equation for the wavefunction in the cluster of interest imbedded in the Madelung field of the remainder of the solid. The eigenvalues $\tilde{\epsilon}_i$ of equation (2.14) or the approximate equation (2.16) represent the eigenvalues ϵ_i of the infinite solid only in the limit that the orbitals ψ_i are localized in the region A.

A basis function expansion is used to determine the unrestricted Hartree-Fock orbitals. Here gaussian type orbitals have been used for this expansion. This type of function offers the advantage of having analytic solutions for the required integrals; however, many such functions are required to achieve the desired accuracy. Cartesian gaussian functions have been used. The spatial part of these functions has the form:

$$\psi(\vec{r}) = \sum_j c_j x^l y^m z^n e^{-\alpha_j r^2}$$

The determination of the gaussian exponents, α_j , for atoms and ions has been the subject of considerable study, and tabulated sets exist in the literature. An all-electron calculation including the core electrons of aluminum and silicon would be impractical, so the ab initio effective potential of Topiol, et al. () is used to replace these core electrons. The integrals are performed using the standard POLYATOM integrals program, and the unrestricted Hartree-Fock calculations are done with the G. T. Surratt program UNFONE.

THE INITIAL ADSORPTION OF OXYGEN ONTO THE
ALUMINUM (100) SURFACE

Aluminum crystalizes in the FCC form, with a lattice constant of 4.05 Å. Aluminum is a metal, and the bulk electronic structure is approximated very well by the "jellium" model. However, attempts to employ this model to describe the local chemisorption process (10) have produced results which are not consistent with experiment (6). Cluster techniques have been used to study the chemisorption process (11,12,40), with results which agree well with experiment if care is taken in choosing the cluster.

Chemisorption is a localized process, and as such the cluster model should provide an accurate description. The difficulties that one encounters here are resultant from the fact that aluminum is a metal, and as such is not well described by a small cluster of atoms (fig. 3.1). One must, therefore, take into account the size of the cluster

used to describe the substrate. These effects will be discussed, along with the binding energy of the oxygen atom for each surface site considered. Calculated one-electron energy levels for these binding sites are compared with the results of photoemission experiments.

3.1 RESULTS OF CALCULATIONS

The positions of the aluminum centers in the clusters are chosen to reproduce the unreconstructed structure of the aluminum (100) surface. It has been assumed here that the lattice does not undergo significant distortions at the surface. This has been shown to be true from comparison of experimental and theoretical LEED studies of clean aluminum surfaces (44).

As possible surface sites for the adsorbed oxygen atom, considered here are the three high-symmetry points of the (100) surface (fig. 3.2). These are a position directly above an aluminum center of the first substrate layer (on-top position); the position central to four aluminum atoms of the first layer, above a second layer atom (hole position); and above (or below) the midpoint of a line connecting two nearest neighbor aluminum centers (bridge position).

The interaction of oxygen with the aluminum surface at the on-top position has been modeled here using two clusters: Al₀, with a single aluminum atom representing the surface; and Al₉O, with five first layer

atoms and four second layer atoms modeling the surface. The binding energy of the oxygen atom to the aluminum surface is shown as a function of its distance above the surface in figure 3.3. For both surface clusters, the equilibrium distance is about 3.5 bohr. The binding energies differ between the two clusters; this energy is 2.25 eV for the Al₁₀ cluster, and 1.36 eV for the Al₁₉O cluster. The charge transfer from the aluminum surface to the oxygen atom is about 0.7 electron in both cases.

For the hole site, the aluminum surface is modeled with two clusters: Al₅O, which has four aluminum centers in the first surface layer, and the central aluminum in the second layer; and Al₉O, which is the Al₅O cluster, to which four additional second layer aluminum centers are added. The importance of including the second layer atoms at this site has been shown by previous theoretical studies of the interaction of oxygen with metal surfaces (45). The oxygen binding energies as a function of the distance above the surface plane are shown for these clusters in figure 3.4. Both clusters have a minimum total energy (maximum binding energy) when the oxygen center is about 0.2 bohr below the plane of the first surface layer. The cluster with only one second layer aluminum atom is found to bind the oxygen adsorbate by 5.4 eV, with a charge transfer to the oxygen of 1.4 electrons. The larger cluster is found to bind the oxygen by 4.8 eV, with a charge transfer of 1.3 electrons to the adsorbed oxygen.

The binding energies computed for this site, as well as those for the bridge site, must be carefully extracted from the calculated total energies. Since the oxygen atom penetrates into the cluster of aluminum centers, the basis functions used to describe the electronic wavefunctions associated with the oxygen adsorbate may improve the description of the substrate electronic structure, thus lowering its total energy. This improvement in the substrate wavefunction can be integrated into the calculation of the binding energy by simply including the basis functions of the oxygen atom when calculating the total energy of the substrate cluster.

The bridge site has been modeled here with three different clusters. The first cluster consists of two nearest neighbor aluminum centers of the surface, and an oxygen atom above the midpoint of the line connecting these centers. The second cluster contains these two centers, as well as two additional centers beneath them from the second aluminum layer. For the final cluster, two aluminum centers from the third layer are added. The inclusion of the deeper layer aluminum centers at this bonding site is necessary because the oxygen atom penetrates the surface, and can move vertically in a "tunnel" between pairs of aluminum centers (see fig. 3.2). The binding energies of an oxygen atom interacting with these aluminum clusters are shown in figure 3.5. For the cluster with two aluminum centers, the oxygen adsorbate is bound 1.3 bohr above the plane of the surface. A charge of 1.25 electrons is transferred to the oxygen atom, which is bound by 3.1 eV. With the inclusion of the two second layer aluminum centers in the

cluster, the equilibrium position of the oxygen center moves to 1.65 bohr beneath the surface, which is just above halfway between the two aluminum layers. The binding energy is found to be 3.8 eV, with a charge transfer of 1.4 electrons to the oxygen. Inclusion of the third aluminum layer produces no significant change in these results; however, this cluster does show that the oxygen center does not want to move deeper into the bulk material, as the total energy of the system is found to be lowest for an oxygen center position just below the first surface layer.

3.2 DISCUSSION OF RESULTS

For the initial stages of adsorption, the oxygen adsorbate is clearly bound below the aluminum surface. The binding is strongest at the hole site. An electric charge of about 1.35 electrons is also transferred to the adsorbed oxygen. These results are in agreement with previously reported work function studies, in which a reported decrease in the work function of the aluminum surface with increasing oxygen exposure (up to one monolayer of coverage) has been attributed to the penetration of negative oxygen ions beneath the aluminum surface (6).

The ultra-violet photoemission spectrum has been reported for low oxygen coverage on the aluminum (100) surface (5); this spectrum is shown in figure 3.6. Also shown is the projected density of states for the oxygen adsorbate previously calculated by Messmer and Salahub (12)

for an oxygen position at the aluminum surface at the hole site. These authors did not calculate the electronic structure for an oxygen position below the surface, nor did they study the interaction of an oxygen adsorbate with any of the other high-symmetry (100) surface sites.

As reported elsewhere (40), the one-electron energy levels of this calculation are in agreement with experiment and previous theory. These energy levels are shown in figure 3.6 for both the hole and bridge sites, with the oxygen position corresponding to the minimum total energy for the cluster. For both sites, the energy levels reported here are those of the largest cluster calculated.

Photoemission experiments studying the aluminum core levels at low oxygen exposures have been reported, with a reported shift in the aluminum 2p energy of 1.3 eV toward lower energy (5). In the present calculation, the shift of the aluminum core levels is found to be 1.1 eV in the same direction. The cause of this core level shift is the electric dipole produced by the charge transfer from the aluminum substrate to the oxygen atom upon adsorption. It has been noted by Flodström, *et al.* that the aluminum core level shift increases to a value of 2.6 eV at higher oxygen exposure (about one monolayer of coverage), thus lowering these orbital energies to the values found in Al_2O_3 . These results are evidence for a two stage oxidation process, with the first step being chemisorption at the hole site, and the second step being incorporation of oxygen beneath the aluminum surface.

The agreement between the calculated one-electron energies for the hole site presented here, along with those of Messmer and Salahub, and reported experimental UPS spectra tend to support the idea that the initial chemisorption of oxygen occurs at the hole site, as one would expect from the binding energies reported in section 3.1.

The hole site is also favored by extended appearance potential fine structure (EAPFS) measurements. Using this technique, den Boer, et al. (4) have reported a nearest neighbor oxygen-aluminum distance of 1.98 Å, or 3.74 bohr. Messmer and Salahub have reported a value of 2.02 Å (3.82 bohr), and the results of the calculations presented here place the oxygen at 1.92 Å (3.63 bohr) from the nearest aluminum center for the hole site. For higher oxygen exposure, den Boer, et al. have reported an experimental value of this nearest neighbor distance of 1.91 Å. This figure is probably an average of the two nearest neighbor spacings found in Al_2O_3 ; these being 1.86 Å (3.51 bohr) and 1.97 Å (3.72 bohr). The longer of these spacings corresponds to oxygen binding at the hole site, while the shorter corresponds to oxygen adsorption at the slightly less energetically favorable bridge site. The present calculation places the nearest neighbor distance at the bridge site at 1.71 Å, or 3.25 bohr.

The results presented above, along with previous theoretical and experimental results, show that for the initial interaction of oxygen with the aluminum (100) surface, chemisorption takes place at the hole site. The present studies have extended previous theoretical understanding of the interaction of oxygen with this surface to include the two additional high-symmetry (100) sites. Work function, UPS, and

EAPFS studies have reported that the nature of this interaction changes when the oxygen coverage approaches one monolayer; the theoretical results presented here lead one to conclude that at this coverage, oxygen begins to adsorb at the bridge site, since the energetically more favorable hole sites are already occupied. The chemisorption of oxygen at the bridge site allows for the incorporation of the oxygen adatoms beneath the aluminum surface at high levels of oxygen exposure, leading to the formation of the oxide Al_2O_3 .

THE ELECTRONIC PROPERTIES OF THE SILICA SURFACE

Silica occurs in six different crystalline forms, as well as the amorphous form. All forms of SiO_2 are based on the SiO_4 tetrahedron, and differ in the Si-O-Si bonding angle. The crystalline form most often studied experimentally is α -quartz, and it is this form which we have used here. α -quartz is hexagonal in structure, with three SiO_2 molecules in each unit cell. The Si-O-Si bond angle is 144° .

The silica surface may be described accurately using a cluster of a small number of atoms. Indeed, calculations on the bulk material () have used the cluster approach. To take into account the effect of the neighboring bulk, appropriate boundary conditions are imposed, as has been discussed in chapter 2. In the case of silica, the cluster is embedded in a point charge array, with the charge transfer determined in a self-consistent manner. This gives the proper electrostatic potential in the region of the surface cluster, and also provides for charge

neutrality. Previous calculations have either employed a free space termination, or imposed periodic boundary conditions which require defects to be present in all unit cells of the crystal.

The clusters used here for the bulk calculations were an SiO₄ tetrahedron, and an Si-O-Si molecule. Both clusters were embedded in a point charge array of 3*3*3 unit cells in size. The calculations of the surface were done using a cluster consisting of the surface silicon atom, its two neighboring oxygen atoms, and the two adjacent silicon atoms to form two joined Si-O-Si molecules. This cluster was embedded in a point charge array of 3*3*2 unit cells. The position of the surface silicon atom was adjusted in order to minimize the total energy. An oxygen atom was then placed above the surface silicon in order to study the surface bonding state.

The one-electron energy levels calculated for the bulk SiO₂ are in good agreement with experiment and previous theory (fig. 4.1). The calculated band gap is 9.4 eV, as compared to 8.9 eV for experiment. The valence band width is calculated to be 9.2 eV, while experimental measurements give about 11 eV. The oxygen 2s band is found at 30.3 eV below the conduction band, while experiment places it 28 eV below. The valence bands are found to be mostly oxygen 2p, with some silicon 3s and 3p character mixed in. This is expected, and agrees with the charge transfer of nearly one-half of an electron from each silicon to each of 4 oxygen atoms, or a configuration of Si²⁺O⁻, as determined by a Mulliken population analysis. This agrees with the observation that silica has both ionic and covalent properties.

For the unreconstructed surface, the E' center is found to have a singly occupied energy level 1.7 eV above the top of the bulk valence band (fig. 4.2). Stephenson and Binkowski () have observed, using XPS, an occupied energy level at 0.75 eV above the bulk valence band edge for samples cleaved in vacuum. They believed this level to be an intrinsic feature of the bulk SiO₂. However, their sampling depth is only about 30 Å, so it is probable that this level is an E' center at or near the surface (). The method of sample preparation which they have used (grinding) could easily have caused these broken bonds to be formed (). It is energetically favorable for an oxygen atom to bind to this surface silicon atom, with a binding energy of 5.1 eV, which is considerably greater than the 2.6 eV per oxygen atom necessary to dissociate molecular oxygen. We shall now turn our attention to this configuration, which is the Si=O surface double bond.

The occupied one-electron energy levels of the surface state are all below the top of the bulk valence band. This is consistent with optical studies, which have found no occupied surface states in the band gap (). The lowering of the valence band can be attributed to the O-Si-O bond angle at the surface being greater than the perfect tetrahedral 109° angle. The bottom of the conduction band for the surface is found to be 4.6 eV below the bulk conduction band edge. The occupied valence surface states can be described as bonding and non-bonding states between the adsorbed oxygen and the surface silicon atom (fig. 4.3a,b). When a surface electron is excited out of the valence band, an anti-bonding orbital (fig. 4.3c) drops out of the

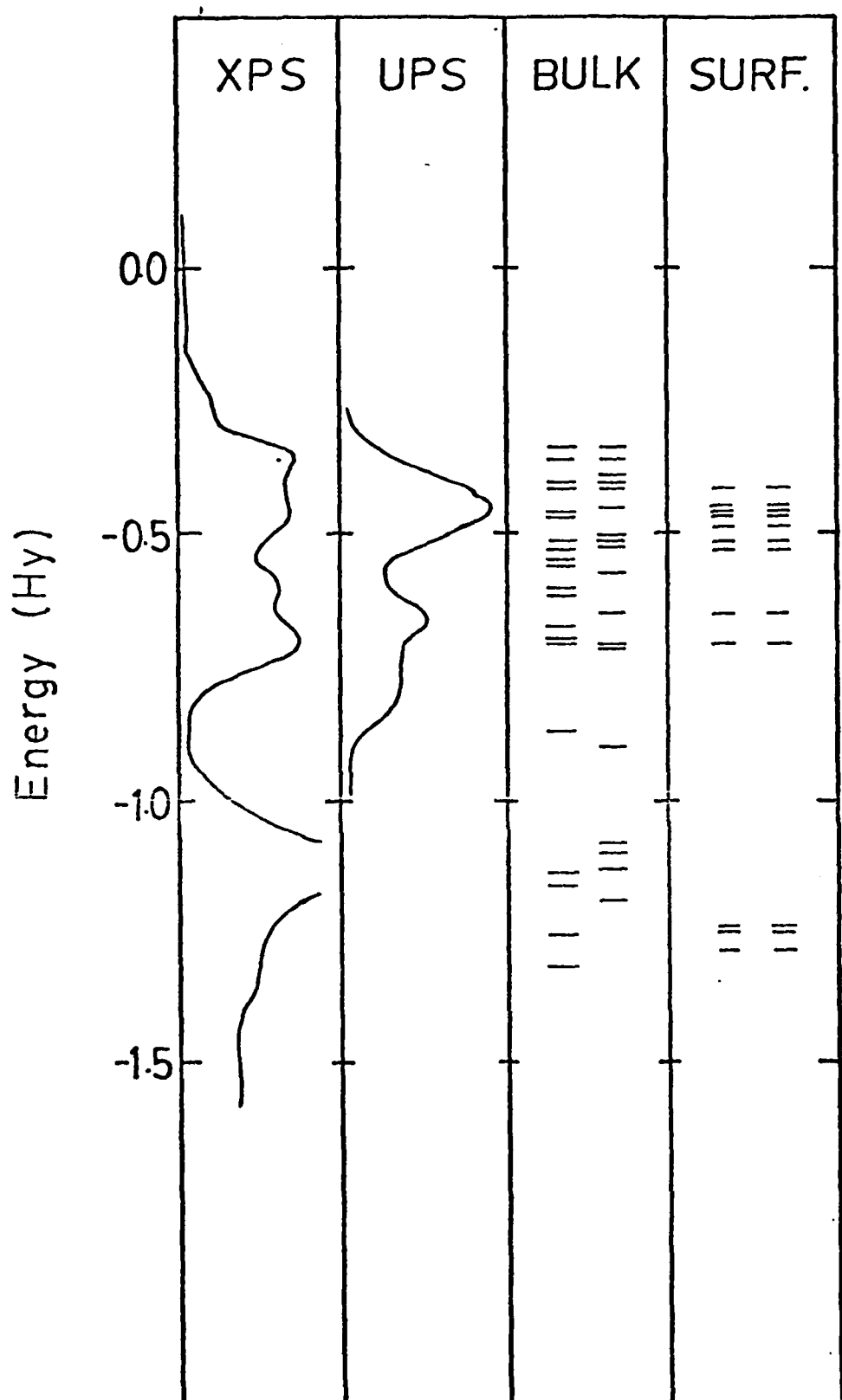
conduction band and is singly occupied. Its energy lowers considerably due to relaxation, and is found at 1.4 eV above the top of the bulk valence band (fig. 4.2). The position of the oxygen atom is 0.1 a. u. farther out from the surface silicon atom for this excited state, relative to its ground state position. This energy difference is in good agreement with Bermudez and Ritz (), and the transition from a non-bonding to an anti-bonding orbital of the surface bond is as they have described. The energy change associated with this transition is 6.1 eV, which is in agreement with the experimental value of 5.0 eV if correlation effects are considered. The 7.4 eV transition can be understood in terms of valence band structure, with transitions from levels in the bonding part of the valence band to the same anti-bonding orbital.

It is noted that this model, the Si=O surface bond, does not predict the surface electronic transition at 3.5 eV that is seen in the second derivative ELS spectra. It has been shown by Gallon and Underwood () that this peak is in fact an artifact of the second derivative mode of detection, and it is not seen in the non-derivative ELS spectrum. They argue that the 3.5 eV peak is produced by the overlap of the "wings" of the primary and the 5.0 eV peaks. The calculations presented here agree with this interpretation.

One remaining point of controversy is the difference between XPS and UPS in describing the top of the valence bands of SiO_2 (fig. 4.4). There exists at this time no agreement as to the cause of this discrepancy. The calculations presented here do, however, favor one

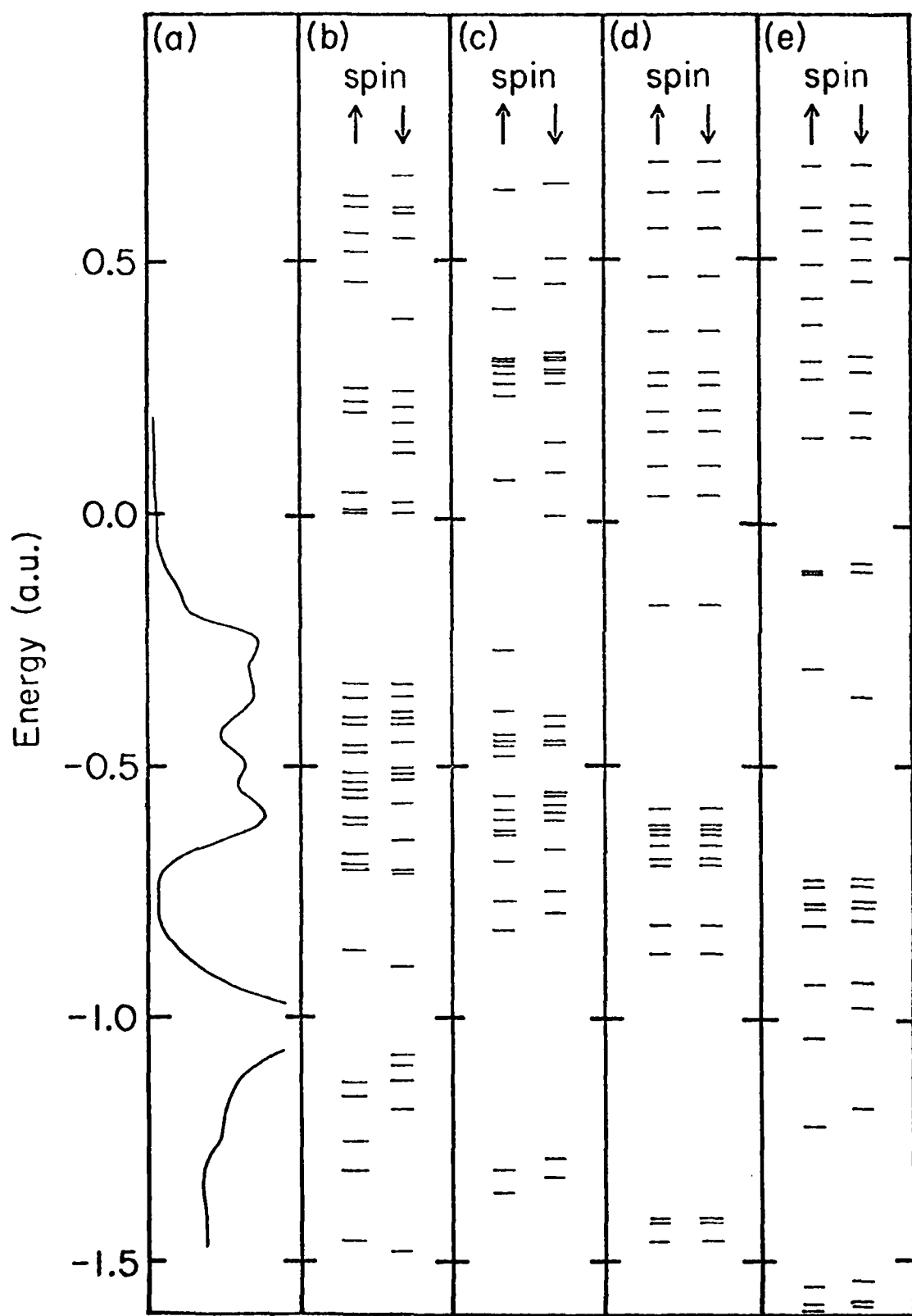
explaination. The two spectra are spatially sensitive to different parts of the sample: XPS is sensitive to the bulk for initial states with small binding energy, while 40.8 eV UPS is surface sensitive. In both the XPS and UPS techniques, the kinetic energy of the photoelectron is sufficiently large that the final state may be approximated by a plane wave. Therefore the difference between the XPS and the UPS spectra must reflect the difference between the bulk and surface valence band densities of states. Comparison between the XPS spectrum and the calculated bulk density of states, and between the UPS spectrum and the calculated surface density of states (for the reconstructed surface) shows that such an explanation does indeed account for the difference in the two spectra (fig. 4.4).

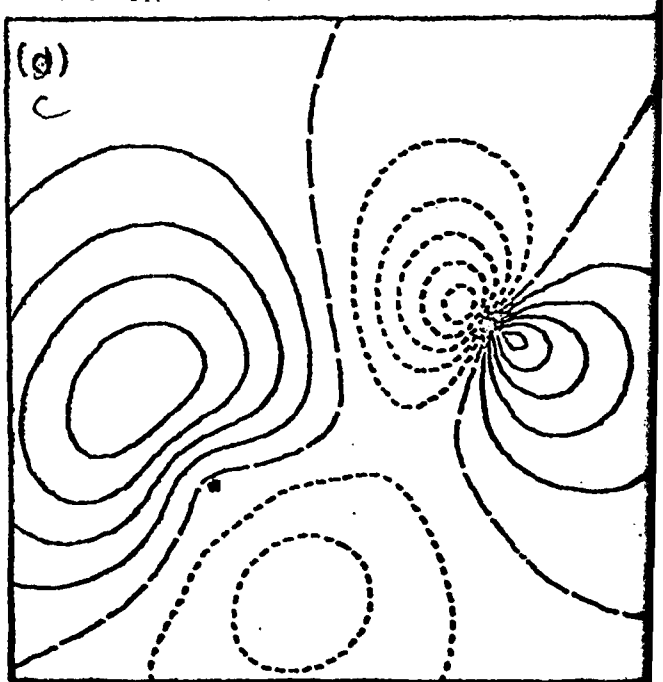
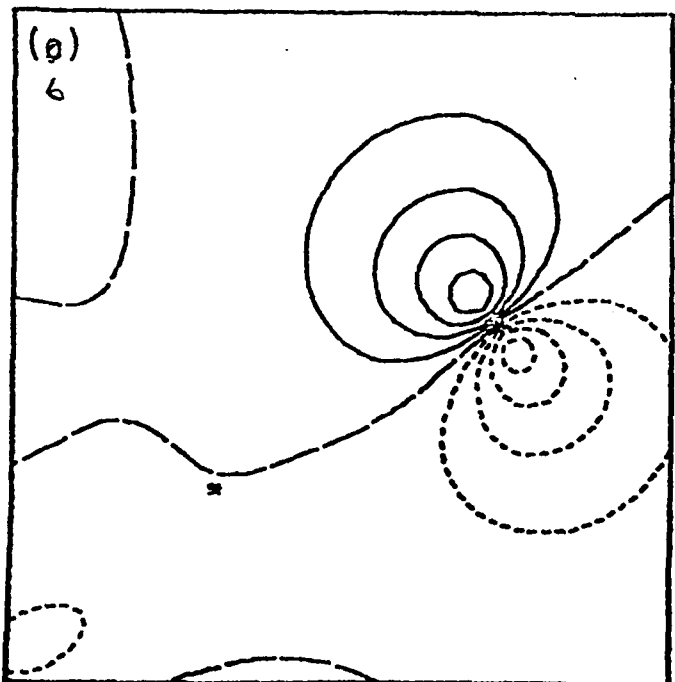
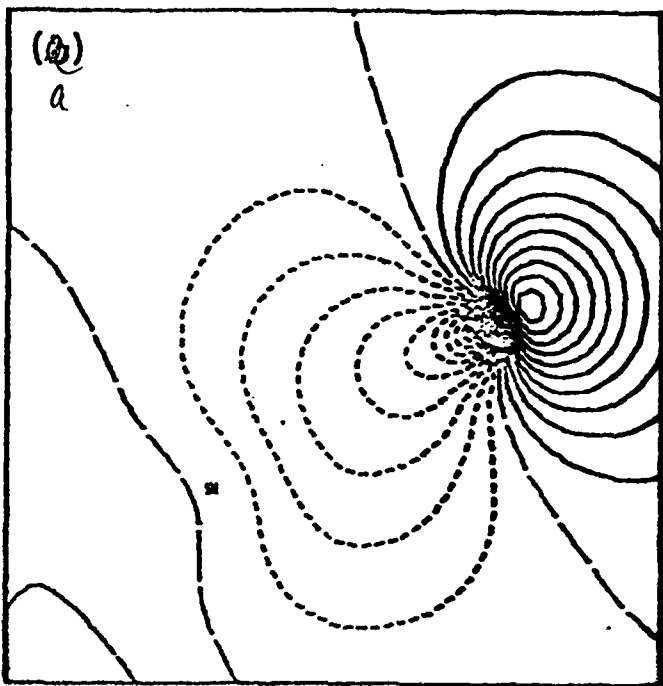
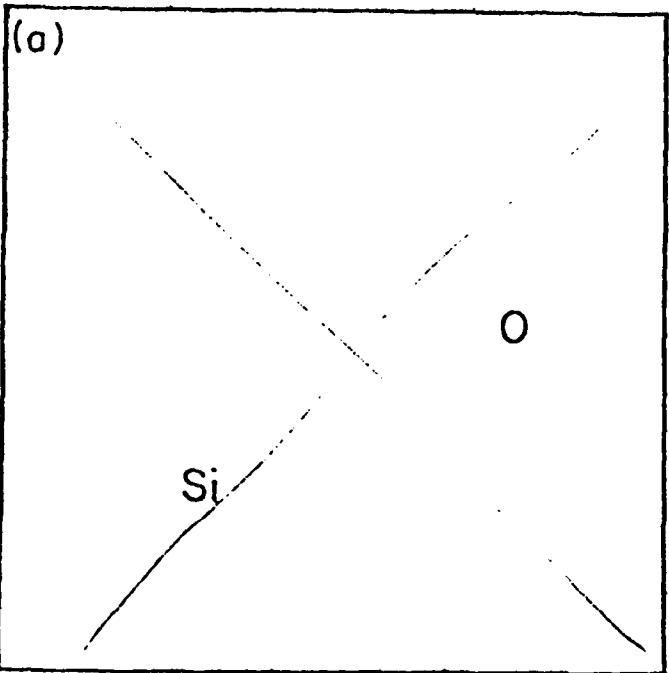
The reconstructed silica surface has been studied in order to determine the nature of the low energy loss ELS peaks. We have found agreement between the theoretically calculated one-electron energy levels presented here and previous experimental results. Of the three models which can account for the peaks, namely a partly oxidized surface region SiO_x , the E'_S center, and the $\text{Si}=\text{O}$ double bond, we conclude that the last is most likely. Support for this conclusion comes from experimental evidence for reconstruction, and from the large binding energy of the oxygen atom to the surface.



Same 2 columns
as Fig 4.1

fig 4.4





4,3

CONCLUSIONS

In this study, the ab initio unrestricted hartree-Fock method has been used to calculate the bulk and surface electronic structure of of silica, and to study the initial interaction of oxygen with the aluminum (100) surface. In both of these materials, the cluster model has been shown to be a useful tool in the calculation of the electronic structures.

In studying the interaction af oxygen with the aluminum (100) surface, the size of the aluminum cluster used had a considerable effect on the results. Since aluminum is a metal, a fairly large cluster of atoms is needed to describe the substrate accurately. That the cluster model worked at all for this calculation is due to the fact that chemisorption is a local process.

It has been shown that an oxygen adsorbate is bound most strongly at the hole site of the clean aluminum surface. The equilibrium position of the adsorbed atom is about 0.2 bohr below the plane of the surface. A charge of 1.3 electrons is transferred from the aluminum substrate to the oxygen adsorbate. This charge transfer creates an electric dipole which causes the aluminum core levels to be shifted downward in energy by 1.1 eV. Previous experiments studying the work function, UPS spectrum, and the EAPFS have reported results for the initial adsorption of oxygen onto this surface which are in agreement with the results of the calculations presented here.

These experimental results have also shown that the nature of the adsorption process changes at about one monolayer of coverage. The theoretical studies reported here lead one to conclude that at this coverage the energetically most favored sites for chemisorption, the hole sites, become fully occupied, and adsorption continues at the bridge site. It is adsorption of oxygen at this site which allows for incorporation of oxygen beneath the aluminum surface, and leads to the formation of the oxide Al_2O_3 .

Also reported here is a study of the bulk and surface electronic structure of silica (α -quartz). The cluster model was again used. The bulk solid and the surface were both modeled with clusters of a few atoms, plus the appropriate boundary conditions. In this case, the boundary condition imposed was a point ion array to provide for charge neutrality and to provide the correct Madelung field.

For the silica bulk, the calculated one-electron energy levels were compared with experimental XPS spectra, and the agreement was found to be excellent, as reported in chapter 4. For the reconstructed silica surface, the structure of the Si=O double bond was found to be the energetically most favorable surface configuration. The electronic structure of this surface bond is able to explain the low energy ELS peaks seen experimentally. This calculations reports a value of 6.1 eV for the lowest energy transition, as compared to 5.0 eV for the experimental result.

Finally, the difference in the reported valence band structures as measured in XPS and UPS experiments is explained. The XPS method is sensitive to the bulk material, while UPS is surface sensitive. Comparison of these spectra with the calculated valence band energy levels shows good agreement between the theory presented here and the experimental spectra.

The ab initio unrestricted Hartree-Fock method, along with the cluster model, has been shown to accurately describe the local electronic properties of many systems. In this report, this method has been shown to be successful in describing the adsorption of oxygen onto the aluminum surface, and in describing the bulk and surface electronic structure of SiO_2 . This technique has also been used to successfully calculate the electronic structure of semiconducting polymers, including defects and impurities (46), and in the description of the excitonic structure of crystalline silicon (47).

Appendix 1 Post Doctoral Associates Supported by this Grant

1. Dr. Chien Hsue, currently National Taiwan University.
2. Dr. G. T. Surratt, currently Bell Labs, Naperville.
3. Dr. D. R. Beck, currently Michigan Technological University.
4. Dr. R. S. Weidman, currently Michigan Technological University.
5. Dr. C. K. Kim, Korean Bureau of Standards.

Appendix 2 Graduate Students Supported by this Grant**All at the Ph.D. level**

<u>Name</u>	<u>Current Occupation</u>	<u>Date of degree (or expected)</u>
R. S. Weidman	Ass. Prof. M.T.U.	June 1980
G. M. Cochran	Tentative General Dynamics	June 1981
K. M. Bedford	U. S. Navy Research Laboratory	June 1981
J. C. Boettger	Research Assistant UIUC	June 1982

Appendix 3 Publications Supported by this Grant

1. A. B. Kunz and M. P. Guse, "The Relationship Between Surface Electronic Structure and Chemisorption of Hydrogen by MgO", *Chem. Phys. Lett.* 45, 18-21 (1977).
2. G. T. Surratt and A. B. Kunz, "Unrestricted Hartree-Fock Calculation for a Cluster Model of NiO", *Sol. St. Comm.*, 23, 555-558 (1977).
3. A. B. Kunz and G. T. Surratt, "A Self-Consistent Energy Band Study of FeO, CoO and NiO", *Sol. St. Comm.* 25, 9-12 (1978).
4. G. T. Surratt and A. B. Kunz, "Theoretical Study of H Chemisorption on NiO Surfaces", *Phys. Rev. Lett.* 40, 347-350 (1978).
5. A. B. Kunz and D. L. Klein, "Unrestricted Hartree-Fock Approach to Cluster Calculations II, Interaction of Cluster and Environment", *Phys. Rev. B* 17, 4614-4619 (1978).
6. C. K. Kim and A. B. Kunz, "Electronic Structure of Silicon with Non-Spherical Potentials for the Two Basis Atoms", *Phys. Stat. Sol. (b)* 87, 795-769 (1978).
7. A. B. Kunz, "Excited States of Transition Metal Oxides" in *Excited States in Quantum Chemistry*, ed. C.A. Nicolaides and D. R. Beck, 471-493 (D. Reidel Co., 1979).
8. H. Itoh and A. B. Kunz, "Theoretical Study of Linear NiCO and CuCO and its implications to Desorption", *Zeit. für Nat.* 36, 114-116 (1979).
9. G. T. Surratt and A. B. Kunz, "Theoretical Study of H Chemisorption on NiO, Perfect surfaces and cation vacancies", *Phys. Rev. B* 19, 2352-2358 (1979).
10. A. B. Kunz and R. S. Weidman, "A Self-Consistent energy-bond study in CuCl", *J. Phys. C* 12, L371-L374 (1979).
11. H. Itoh and A. B. Kunz, "Molecular Orbital Study of Interactions of Single Transition Metal Atoms with PF₃ and CO Ligands", *Chem. Phys. Lett.* 64, 576-578 (1979).
12. H. Itoh and A. B. Kunz, "Molecular Orbital Calculations of Carbonyl Compounds of Ni and Cu", *Fund. Res. in Honno. Cat.* 3, 73-82 (1979).
13. D. L. Klein, G. T. Surratt and A. B. Kunz, "Unrestricted Hartree-Fock Calculations for a Cluster Model of CoO", *J. Phys. C* 12, 3913-3919 (1979).
14. A. B. Kunz, R. S. Weidman and T. C. Collins, "Electronic and Transport Properties of CuCl", *Int. J. Quant. Chem. S* 13, 453-465 (1979).
15. A. B. Kunz, "Cluster Chemisorption", *Topics in Current Physics* 19, 115-147 (1980).

16. G. G. Wepfer, G. T. Surratt, R. S. Weidman and A. B. Kunz, "Theoretical Study of H Chemisorption on NiO, II, Surface and Second-layer Defects", Phys. Rev. 21, 2596-2601 (1980).
17. T. C. Collins, A. B. Kunz and R. S. Weidman, "A Model for the Diamagnetic Anomaly in CuCl", Lect. Notes in Phys. 113, 240-254, (1980).
18. A. B. Kunz and D. M. Ginsberg, "Band Calculation of the Effect of Magnetic Impurity Atoms on the Properties of Superconductivity", Phys. Rev. 13 22, 3165-3172 (1980).
19. A. B. Kunz and J. T. Waler, "Positron and Electron Energy Bands in Several Ionic Crystals Using Restricted Hartree-Fock Methods", Sol. St. Comm. accepted.
20. A. B. Kunz and T. O. Woodruff, "Some Highly Excited States of the LiH Molecule: Calculations Relevant to Core-Hole Initiated Relaxation Process (CHIRP'S) in Ionic Crystals", Sol. St. Comm. accepted.
21. A. B. Kunz, "Electronic Structure of NiO", J. Phys. C. accepted.
22. A. B. Kunz, "Properties of Narrow Band Insulators", Int. J. Quant. Chem. accepted.
23. K. L. Bedford and A. B. Kunz, "Ab Initio Studies of the Initial Adsorption of Oxygen onto the Aluminum (100) surface", in preparation.
24. J. C. Boettger and A. B. Kunz, "Ab Initio Energy Bands and Ionization Energies for AlP, GaP and GaAs", in preparation.